

AUTOMATIC ROAD EXTRACTION FROM HIGH RESOLUTION SATELLITE IMAGERY

Thesis submitted in partial fulfillment
of the requirements for the degree of

MASTER OF SCIENCE
in
COMPUTER SCIENCE AND ENGINEERING

by

VINAY PANDIT
200707036
vinaypandit@research.iiit.ac.in



LAB FOR SPATIAL INFORMATICS
International Institute of Information Technology
Hyderabad - 500 032, INDIA
DECEMBER 2009

Copyright © VINAY PANDIT, 2009

All Rights Reserved

International Institute of Information Technology
Hyderabad, India

CERTIFICATE

It is certified that the work contained in this thesis, titled “Automatic Road Extraction From High Resolution Satellite Imagery” by VINAY PANDIT, has been carried out under my supervision and is not submitted elsewhere for a degree.

Date

Adviser: Dr. K. S. RAJAN

To My Parents

Acknowledgments

First and foremost, I would like to express gratitude to my advisor, Dr. K. S. Rajan, for his guidance, suggestions, support and encouragement throughout this research work. I am thankful to him for creating excellent environment for me to “make and break” various ideas and concepts. During this research I am greatly benefited from his immense knowledge and vast research experience.

I would like to thank NDC and NRSC Hyderabad for providing CARTOSAT-2 imageries for carrying out this research. Especially, I would like to thank Dr. R. Nagaraja and Dr. N. Aparna of NRSC Hyderabad for their guidance and support during this research work.

My thanks to all my friends in IIIT who made last two years most memorable and joyful. My thanks to my senior friend Keerthiram for being “answer bank” to my uncountable number of queries. One of the key ideas presented in this thesis took its shape during a discussion with Keerthiram.

I am thankful to my parents for their endless love and patient support all these years. I know that my decision to re-enter student life has introduced tremendous pressure on them. I am also thankful to my sister for forgiving me for not keeping up my promise to support her education.

Abstract

An accurate and up-to-date road network database is essential for GIS (Geographic Information System) based applications such as urban and rural planning, transportation management, vehicle navigation, emergency response, etc. Often, road database is generated through field surveys with the help of GPS (Global Positioning System) enabled instruments. This approach of road extraction, however, is time consuming and labour intensive. With increase in availability of satellite imagery both in high and low resolutions, automatic road network extraction from satellite imagery has received considerable attention and has been studied extensively since 1970s. Since road region appear as linear segment in low resolution images, earlier research on road extraction focused on extracting road center-line from low resolution images. On the other hand, high resolution satellite images provide an opportunity to extract entire road area, which are particularly useful for vehicle navigation, along with road network. However, factors like occlusion due to trees along the road, building shadows and vehicles, variation in road surface characteristics (example, bitumen road versus concrete road) and changing road geometry, which become more apparent in high resolution satellite images, make road extraction a challenging problem.

Though several road extraction techniques have been proposed in the literature, because of various assumptions about the road region characteristics and imaging modality, such techniques often exhibit limited success in the real scenarios. Of these techniques, the region growing based road extraction approach, in which road extraction starts with road seed points (either provided manually or generated automatically) and extracts entire road region based on predefined matching criteria, holds considerable promise. In this thesis we present a novel automatic road extraction algorithm based on adaptive texture matching (ATM-R), which is a variant of region growing approach. The algorithm developed in this thesis is robust to variations in radiometric resolution of input images, road surface characteristics (texture) and road geometry and is scalable to inputs from different sensors. In the proposed algorithm, difference in a pair of closely dated multi-temporal images of same geographic area has been studied to generate road templates (seeds) and such templates are further utilized to extract remaining road region within a road template matching framework which adapts to local road texture.

To assess the performance of the proposed algorithm, a set of images encompassing wide range of radiometric resolutions and different spatial resolutions were prepared. The image set consisted of grayscale equivalent of pan-sharpened IKONOS images, panchromatic CARTOSAT-2 images and grayscale equivalent of images captured from Google Earth. Images were chosen to include road regions

with varying width, wide range of road surface reflectance values and different textures. Experiments were conducted on images with disconnected road segments, multi-lane roads, road regions occluded with trees and images with road over-bridges. The measures used to evaluate the algorithm performance are road network completeness, road area completeness and correctness of road area. The algorithm is able to consistently extract 70% to 90% of the road network and has a high performance against all the three measures.

Along with generating road network the proposed algorithm is able to extract road area which can be further used to assess road width, number of road lanes and other auxiliary road network information. The algorithm has considerably reduced manual intervention in road extraction process and avoided the need for GCPs (ground control points).

Contents

Chapter	Page
1 Introduction	1
1.1 Road Region Properties in Satellite Images	2
1.1.1 Spectral Properties	2
1.1.2 Spatial Properties	2
1.1.3 Geometric Properties	3
1.1.4 Topological Properties	3
1.1.5 Contextual Properties	3
1.2 Thesis Objective	3
1.3 Thesis Organization	4
2 Related Works	5
2.1 Road Extraction Techniques	5
2.2 Road Seed Extraction Techniques	7
2.3 Discussion	8
3 Automatic Road Seed Extraction Using Multitemporal Satellite Images	9
3.1 Road Seed Extraction Using Miltitemporal Images	9
3.1.1 Road Seed Characteristics	10
3.1.2 Role of Multi-temporal Satellite Imagery	10
3.1.3 Automatic Road Seed Extraction	10
3.2 Road Extraction	12
3.3 Results	12
3.4 Discussion	13
4 Adaptive Texture Matching For Road Extraction	15
4.1 Road Extraction Algorithm	16
4.1.1 Framework for Road Extraction	16
4.1.2 Choice of Image Features and Distance Functions	19
4.1.2.1 Contrast	19
4.1.2.2 k-means Based Features and Distance Function	20
4.1.2.3 Histogram and Histogram Quadratic Distance	20
4.1.2.4 Directionality	21
4.1.3 Orientation of Road Regions	21
4.1.4 Road Intersections	22
4.1.5 Initialization in case of manual seeds	22

4.2	Results and Evaluation	23
4.2.1	Data	23
4.2.2	Evaluation Measures	24
4.2.2.1	Road Network Completeness	24
4.2.2.2	Road Area Completeness	25
4.2.2.3	Correctness of ERA	25
4.2.3	Results and Discussion	26
4.3	Discussion	30
5	Road Extraction System	31
5.1	System Block Diagram	32
5.2	Results	33
5.3	Other Potential Applications of Multi-temporal Images	34
5.3.1	Rail Network Extraction	34
5.3.2	Defense Applications	35
5.3.3	Monitoring Large Infrastructure	35
5.3.4	Extracting Large Water Bodies	36
5.4	Discussion	36
6	Conclusions	37
<i>Appendix A: Image Specifications</i>		39
A.1	CARTOSAT-2	39
A.2	IKONOS	39
A.3	Google Earth	40
Bibliography		42

List of Figures

Figure	Page
1.1 Variation of road characteristics within an image	2
1.2 Variation of road characteristics across different satellite images	3
3.1 Working of vehicle detection algorithm	11
3.2 Result of road extraction on pair 2	13
3.3 Result of road extraction on pair 3	14
4.1 Block diagram of proposed ATM-R algorithm	16
4.2 A representation of road region	17
4.3 Proposed road extraction framework	17
4.4 Suitability of selected features	19
4.5 Road intersection detection	21
4.6 Selecting reference road region	22
4.7 The ATM-R road extraction result on IKONOS input	23
4.8 The ATM-R road extraction result on IKONOS input	24
4.9 The ATM-R road extraction result on IKONOS input	26
4.10 The ATM-R road extraction result on IKONOS input	26
4.11 The ATM-R road extraction result on IKONOS input	27
4.12 The ATM-R road extraction result on CARTOSAT-2 input	27
4.13 The ATM-R road extraction result on CARTOSAT-2 input	28
4.14 The ATM-R road extraction result on Google Earth input	28
4.15 Road extraction accuracies for various widths of reference road region	28
4.16 The ATM-R road extraction result on Google Earth input	29
5.1 Road Extraction System Block Diagram	31
5.2 Result of road extraction system	34
5.3 Result of road extraction system	34
5.4 Train detection result	35

List of Tables

Table	Page
2.1 Road extraction methods	7
3.1 Choice of threshold range	12
4.1 Choice of image features	18
4.2 Images used in our experiments	23
4.3 Performance of proposed algorithm	25
4.4 Performance comparison with Fourier descriptor based method	29
A.1 Image Specifications	40

Chapter 1

Introduction

The road network is an essential geographic information system (GIS) layer in applications such as urban and rural planning, transportation management, vehicle navigation, emergency response, etc. Rapidly changing urban environments accelerate the need for frequent updates or revisions of road network databases. Other utilities of road network include registration with multi-temporal images for change detection, automatically aligning two spatial datasets, etc. Often road database is generated through field surveys with the help of GPS (Global Positioning System) enabled instruments. Manually delineating road network from high resolution satellite imagery is another widely adopted road network generation approach. Automatic road extraction systems, which move away from these time consuming and logically challenging process of driving along roads to register road points and error prone manual delineation approach, can be instrumental in generating road network rapidly and accurately. Particularly, automatic road network extraction using high resolution satellite imagery can be cost effective in rural areas and other remote and inaccessible geographic areas.

Extreme complexity of an urban scene poses many challenges for automated urban road network extraction. The difficulties in automated road network extraction from remotely-sensed imagery lie in the fact that the image characteristics of road feature vary a lot according to sensor type, spectral and spatial resolution, ground characteristics, etc [1]. Even in the same image, different roads often appear differently (See Fig. 1.1). In urban residential areas, with high resolution remotely-sensed image, the situation becomes even worse. With high resolution satellite images road extraction algorithm can accurately localize the road sides along with extracting road network. But meanwhile, occlusions due to vehicles and trees along the road will also become more apparent [2]. Difference in surface characteristics of different road segments in a single image too becomes obvious in higher resolutions. Substantial amount of research has been carried out to extract road network from satellite imagery in the photogrammetric and computer vision communities. Though several road extraction techniques have been proposed in the past, because of various assumptions about the road region characteristics and imaging modality, such techniques often exhibit limited success in the real scenarios.

As stated in [3], the study of road region characteristics, their changes with respect to geographic background, image types, image resolutions, development of mathematical models to represent these

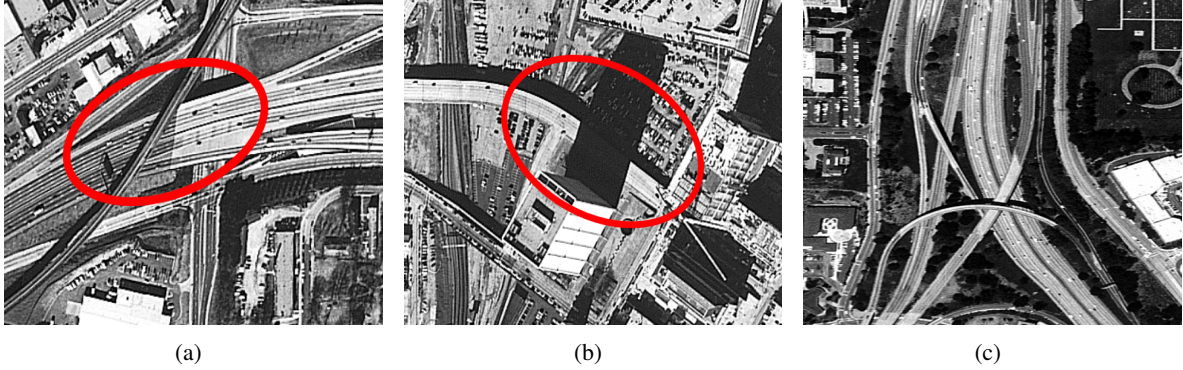


Figure 1.1 Variation of road characteristics within an image. (a) A scenario where road reflectance values change sharply (marked with a ellipse), (b) a scenario where road region is occluded by building shadow (marked with a ellipse), and (c) sample road region where road width and curvature vary significantly.

characteristics, are critical in order to make substantive progress in this area. In [4] *road* is defined to be geometrically a long and continuous object with narrow width, to be radiometrically an object made up of slowly varying grayscale and texture and to be spectrally an object with material dependent consistent signature. However, in practical scenarios since a road extraction algorithm can consider only a limited set of characteristics when these characteristics change beyond a limit, the algorithm may fail [1].

1.1 Road Region Properties in Satellite Images

1.1.1 Spectral Properties

Although it depends on the pavement materials used to construct road, in general, in gray scale images, road region can be assumed to be predominantly bright regions or predominantly dark regions with contrasting surrounding. However due to the variety of sensing conditions and road conditions, the reflectivity values (or the digital numbers) are hardly to be compared directly. Also, in real scenarios road reflectivity values are subjected to a range of noises and artifacts. In Fig. 1.2, variation in road reflectance values across different satellite images is evident.

1.1.2 Spatial Properties

Spatially, road region extends along the road direction continuously and narrowly. In low-resolution images, road may appear as a line. In high-resolution images, road region appears as elongated regions with parallel borders. This property can be used to separate road regions from many other spectrally similar objects, such as parking lots, buildings, crop fields as these non-road objects usually occupy a large and wide area.

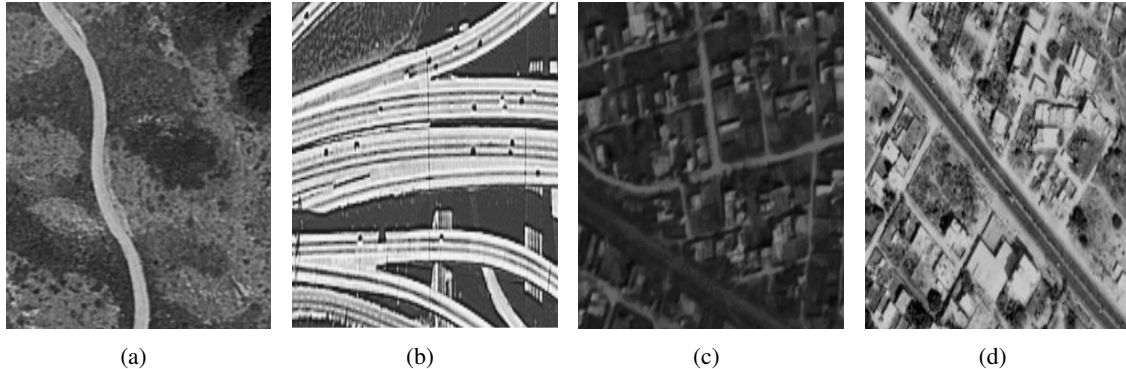


Figure 1.2 Variation of road characteristics across different satellite images. (a) Road region in an IKONOS image, (b) road region with significantly different texture in a IKONOS image, (c) road region in a CARTOSAT-2 image, and (d) road region in typical Google Earth screen capture. Road region in IKONOS images appear brighter than that in Google Earth screen capture.

1.1.3 Geometric Properties

A road network usually has an upper bound in local curvature which follows from smooth traffic flow requirement. However road width may change significantly in given image (See Fig. 1.1(c)). These geometric properties justify extracting road primitives locally and then linking them to form a road network.

1.1.4 Topological Properties

Roads are built to link certain places together and neighboring roads are connected to form networks. This property is usually used in the road network formation step, particularly when bridging gaps.

1.1.5 Contextual Properties

The type of road is one of the contextual properties which can be used in road network extraction. In the real world, road regions have different classes, such as highway, driveway, pathway, etc. Therefore knowing the types of the roads under consideration can be a helpful hint in determining the parameters used, e.g. the width of a search window. This information can also be used to verify the extracted road properties, e.g. the road width [1].

1.2 Thesis Objective

In this thesis, we will present a robust automatic road extraction system which addresses following challenges in road extraction:

- varying radiometric and spectral resolution of input image

- varying road surface characteristics (texture)
- varying road widths and curvatures
- road occlusion due to trees along the road, building shadows and vehicles
- false detection due to objects sharing similar spectral characteristics of road region.

In the proposed algorithm, difference in a pair of closely dated multi-temporal images of same geographic area has been studied to generate road templates (seeds) and such templates are further utilized to extract remaining road region within a road template matching framework which adapts to local road texture. We have used grayscale equivalent of pan-sharpened IKONOS images, panchromatic (grayscale) CARTOSAT-2 images and grayscale equivalent of images captured from Google Earth to assess the performance of the proposed algorithm. Images were chosen to include road regions with varying width, wide range of road surface reflectance values and different textures. Experiments were conducted on images with disconnected road segments, multi-lane roads, road regions occluded with trees and images with road over-bridges. The measures used to evaluate the algorithm performance are road network completeness, road area completeness and correctness of road area. The algorithm is able to consistently extract 70% to 90% of the road network and has a high performance against all the three measures.

1.3 Thesis Organization

The thesis is organized as follows. In chapter 2 a brief literature survey of research work related road extraction is provided. Chapter 3 introduces an automatic road seed extraction algorithm using multi-temporal satellite images. A semi-automatic road extraction algorithm based on texture matching is presented in chapter 4. A complete road extraction system based on road seed extraction algorithm of chapter 3 and road extraction algorithm of chapter 4 is presented in chapter 5. Conclusions and a discussion on scope for future work is provided in chapter 6.

Chapter 2

Related Works

Research on extracting roads from aerial and satellite images can be traced back to the 1970s [5]. The classification of surveys and different techniques on automatic and semi-automatic road extraction methods and related works is very difficult, given the variety of existing proposals in the literature. Proposed methods vary in 1) target input image type (aerial vs satellite images, low resolution vs high resolution images, panchromatic vs multi-spectral/multi-band images), 2) scene type (rural vs urban), 3) level of required manual interaction (automatic vs semiautomatic) 4) road model used (road as linear object vs road as ridge) and 5) methodology used (segmentation vs road tracking). Detailed discussion on various road extraction techniques has been presented in [4], [7] and [8]. This chapter first briefly summarizes the work of [4] and [7] and then gives detailed account of recent trends in road extraction techniques. Most of the road extraction techniques require road reference points, referred as road seeds, which is either provided manually or detected automatically. Fully automatic road extraction system will need to detect road seed points automatically along with automatically extracting road network. In this chapter we will also discuss various automatic road seed extraction techniques proposed in the literature.

2.1 Road Extraction Techniques

In [4], the author discusses various feature extraction techniques utilized in road detection and extraction from aerial and satellite imagery and evaluates them with respect to methodology, strengths, drawbacks, and implementation approach. The techniques were categorized based on four different phases of road detection, 1) road region finding, 2) road shaping, 3) road linking and 4) thinning and vectorizing. The survey summarizes that, edge detection techniques, watershed transform and wavelet transform which utilize radiometric or spectral information content are used in road region finding phase. Parallel edge detection filters and road template matching which utilize radiometric or spatial information content are used for road shaping. Road linking is achieved using Hough transform, optimal search, direction filters and using LIDAR (Light Detection And Ranging) data. Finally, techniques like self-

organizing map, snakes, and template matching are used in thinning and vectorizing phase of road detection.

In [7], the author presents a bibliography of nearly 250 references relevant to road extraction from aerial and satellite imagery. Different techniques are first categorized based on the preset objective, the extraction technique applied, and the type of sensor utilized. The road extraction techniques are further classified into 8 different categories including, road tracking methods, morphology based techniques, segmentation and classification based methods and multi-scale and multi-resolution based techniques.

Of the recent road extraction techniques, [9] presents a semi automatic road extraction scheme which uses a-trous algorithm to locate and identify road pixels and graph searching algorithm [10], which takes start and stop point from the user, to draw a final complete road network. The method is successful in identifying road pixels and hence to reduce the search space. However, a large number of non-road pixels are also labeled as road pixels and hence the method can not easily be automated. The technique in [11] models road in Synthetic Aperture Radar (SAR) image as a homogeneous dark area bounded by two parallel boundaries. Candidate road region are first detected using Gaussian probability iteration segmentation [12] and then the road is detected using Average Hough Transform. Semiautomatic method in [13] makes use of edge information along with texture and color information to extract roads in high-resolution satellite images. A Bayesian tracking framework in [14] makes use of the particle filter, a technique for implementing a recursive Bayesian filter by Monte Carlo simulations, for the road tracking, where local linear feature and global contextual knowledge are incorporated into the filtering procedure. An automatic method in [1] first segments the image using k-means clustering and then road cluster is identified using fuzzy classifier. The method in [15] makes use of region competition [16] approach in which a initial model, a centerline and its parallel copies to each road side, is deformed by using region growing techniques to obtain a rough road approximation. This model is then refined by region competition. This approach is appropriate given that the majority of the roads have two important characteristics: in a small portion of road the radiometry and curvature changes are small.

A fully automatic road extraction technique in [17] uses a-trous algorithm with two different wavelet bases to denoise the input image. Since the prominent features appear in both the wavelet transformed images but not noise, resulting images are fused using PCA to denoise the input image. Road detection is then carried using fuzzy logic algorithm with the help of linguistic variables namely, mean, standard deviation computed over a 5x5 window. Since the algorithm require an estimate of bounding values for linguistic variables, the algorithm is dependent on radiometric values of road region. The Fourier shape descriptor based method in [18] defines a local homogeneous region around a pixel enclosed by a polygon is the pixel footprint and it is represented as distance function between the center pixel and pixels on the enclosing polygon. Fourier descriptors are computed on these distances and road tracking is continued in the direction of dominating peaks of resulting function. Improved algorithm in [19] introduced the road tree pruning step which makes use of a Bayes decision model based on the area-to-perimeter ratio of the footprint to prune the paths that leak into the surroundings. However, presence of noise in the road region can result in non-rectangular footprints producing inaccurate road extraction

Author	Input Type	Scene Type	User Interac-tion	Methodology
Udomhunsakul [9]	Low resolution, panchro-matic satellite image	Rural	Semiautomatic	Segmentation
Cheng-Li [11]	High Resolution, panchro-matic satellite image	Rural	Automatic	Segmentation
Xiao [13]	High Resolution, multi-spectral satellite image (IKONOS)	Urban	Semiautomatic	Road track-ing
Zhang [1]	High Resolution, multi-spectral satellite image (Quickbird)	Urban	Automatic	Segmentation
Amo [15]	High resolution aerial image	Urban	Semiautomatic	Road track-ing
Tuncer [17]	High Resolution, panchro-matic satellite image	Urban	Automatic	Segmentation
Hu [18]	High Resolution, panchro-matic satellite image	Urban	Automatic	Road track-ing
Christophe [20]	High Resolution, panchro-matic satellite image (Quickbird)	Urban	Automatic	Segmentation
Grote [21]	High resolution aerial image	Urban	Automatic	Segmentation

Table 2.1 Different Road extraction methods and their classification

results. The method in [20] makes use of high resolution multi-spectral images for road extraction. The method treats each pixel as a vector and computes spectral angle at each pixel and line detection is carried out in spectral angle image. Line linking is carried out later to address line disconnection due to tree and shadow along the road. The method has generated considerable amount of false detection at buildings. The method in [21] first segments image into small segments using normalized cuts [22] and such segments are then combined to form larger segments according to color and edge criteria. Further, generated larger segments split based on branches of their skeletons and shape criteria is used to extract road parts. Road extraction techniques discussed in this section are summarized in Table 2.1.

2.2 Road Seed Extraction Techniques

Fully automatic methods attempt to completely circumvent human intervention during the extraction process, in which two basic steps can be identified: road seed extraction and road network completion [6]. In automatic road seed extraction road seeds are found by analyzing whole image for pre-defined local road properties or features [23]. In [24], a new shape based feature vector, symmetrical edge orientation histogram, has been introduced to detect road seeds. The method is based on the following hypothesis about main roads, (1) boundaries of road, vehicles, markings and pavements compose a set

of parallel line segments and hence in an appropriately sized patch including main roads, there will be a major part of edge pixels with identical gradient orientation, (2) along the gradient orientation of an edge pixel of a main road, another symmetrical neighboring edge pixel with almost identical orientation can be found. The method in [6] is based on a set of four road objects and another set of connection rules among road objects. Each road object is a local representation of an approximately straight road fragment and its construction is based on a combination of polygons describing all relevant image edges, according to some rules embodying road knowledge. Each one of the road seeds is composed of a sequence of connected road objects, in which each sequence of this type can be geometrically structured as a chain of contiguous quadrilaterals. In [18] any rectangular region with a narrow width is considered as road segment. Area enclosed in pixel footprint (explained in previous section) around each pixel is compared with ideal rectangular footprints and if the ratio is less than a predefined threshold then such pixels are considered as road seeds. For each such seed further road extraction is carried out. From the experiments reported in [19] it is clear that the process generates large number of road seeds. Since buildings too are rectangular considerable number of false detection is also observed. Also, since each pixel is tested for road pixel the method is computationally expensive.

2.3 Discussion

In this chapter we have discussed various approaches adapted to extract road network. We have also analyzed the input types suitable for such approaches and discussed possible limitations of the techniques. Though several techniques exists for road extraction, a completely automatic road extraction system which can function independent of input type and complexity has not been realized. In coming chapters we will attempt to develop a road extraction system which will address most of the challenges in automatic road extraction.

Chapter 3

Automatic Road Seed Extraction Using Multitemporal Satellite Images

Road tracking is a popular road extraction technique. Road trackers generally need a starting pixel on the road (seed) and another pixel to define the direction of the road, and grow iteratively by searching for and adding road segments. A spanning tree of the road network is formed by some process that uses local information to add new segments to the graph based on the pixel intensities of the image [18]. Most of the existing road tracking algorithm extract road starting with manually provided road seed points. However, a fully automatic road extraction system will need to detect road seed points automatically along with automatically extracting road network. In this chapter we will develop an automatic road seed extraction algorithm. The motivation is the fundamental importance of road seeds for the subsequent phase. The potential success of road network completion strategies is significantly determined by the quality of the results of the first phase [6]. Road seed extraction presented in this chapter is based on method presented in [25], which exploits temporal variations in closely dated images. Utility of the detected road seeds is demonstrated using Fourier descriptor based road tracking algorithm developed by *Hu et al* [18]. Results of experiments carried out on CARTOSAT-2 imageries are discussed.

3.1 Road Seed Extraction Using Multitemporal Images

To understand the evolution and importance of the road seed extraction algorithm presented in this chapter, first we need to have closer look at challenges in road extraction from satellite images. Challenges in road extraction from satellite images are,

- varying radiometric and spectral resolution of input image
- varying road surface characteristics (texture)
- varying road widths and curvatures
- road occlusion due to trees along the road, building shadows and vehicles
- false detection due to objects sharing similar spectral characteristics of road region.

Often, road tracking algorithm fail (stop abruptly) upon encountering obstacles like vehicles on the road. Moving away from this popular thought, method in [25] utilizes vehicles on the road as clue for existence of road region. Once the vehicles are detected we can detect the road seed points in the neighborhood of detected vehicles. Before going to the actual details of road seed extraction, we will discuss various characteristics of road seeds.

3.1.1 Road Seed Characteristics

Often the whole image is tested for local road property, and road seeds are found. Usually, the local road properties tested are geometric (Example: road regions are smooth), radiometric (Example: road regions usually have contrasting background) and shape (Example: road regions are rectangular region with a narrow width) [6]. The results of this step are the road seeds or a fragmented road network. Detailed discussion on various existing road seed extraction techniques can be found in Chapter 2.

3.1.2 Role of Multi-temporal Satellite Imagery

The revisit capabilities of modern remote sensing satellites provide temporal data that can convey valuable information. Since the variation in the closely dated images (especially in urban areas) is minimal, such images are not much used in change studies. The difference between two consecutive revisits can be a major cue of the location of non-stationary objects like vehicles on the road and that is the central theme of this chapter.

Vehicle detection can aid road extraction in two aspects: 1) finding road seed points 2) enhancing the homogeneity of road region in the image. However, multi-temporal images pose newer challenges for road seed extraction. In a pair of multi-temporal images the difference image, obtained by finding the difference between the pair, is expected to indicate the presence of the non-stationary objects like vehicles. However, because of difference in sun elevation angle, misalignment due to geometric distortion and other atmospheric phenomenon (existence of cloud etc), there will be a variation in the reflectance values across the input image pair. The difference in sun elevation angle also results in variation of shape and shift in location of shadows of the objects in the scene. Presence of non-stationary objects other than vehicles is another important challenge.

3.1.3 Automatic Road Seed Extraction

In high resolution satellite images, vehicles can be modeled as a small region consisting of pixels of uniform intensity (either all bright or all dark). For the purpose of generating road seed points for road tracking, detection of bright vehicle pixels in the background of road region consisting of dark pixels (or dark vehicle pixels in the background of bright road pixels) shall suffice. Most important aspect of our vehicle model is based on observation that the vehicles are visible in only one of the two input images.

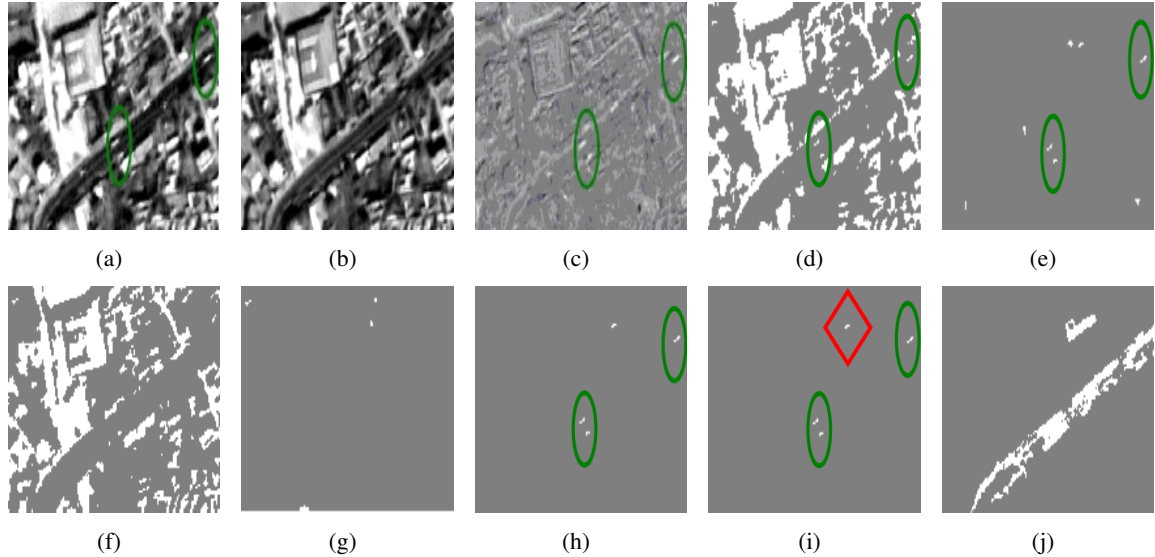


Figure 3.1 Working of vehicle detection algorithm on the first image pair. (a), (b) Original image pair. (c) The difference image. (d), (f) Binary filtered image for image1 and image2. (e), (g) Area thresholded image for image1 and image2. (h) Image after discarding objects of similar intensity values. (i) Vehicle detection result. Ovals show detected vehicles and rhombus shows false positive. (j) Road extraction result.

Area Threshold:

Our vehicle detection algorithm starts with thresholding both the input images with threshold *white_th* to retain bright pixels. The search space is further reduced by first identifying 8-connected pixels as objects and then discarding objects with area smaller than a threshold *min_area* and area larger than a threshold *max_area*.

Handling Misalignment Due to Geometric Distortion:

In the resultant area thresholded images, in case of objects which are vehicles, we can expect road region at corresponding pixel co-ordinates of the complementary image. Hence, objects with average value of absolute difference between corresponding pixels less than a threshold, *diff_th*, are discarded. At this stage, because of marginal misalignment between two images (due to geometric distortion), bright non-vehicle objects will also exhibit significant difference between corresponding pixel values. In the area thresholded images, however, such non-vehicle objects will have an overlapping area and hence can be identified and can be discarded. The remaining objects are tagged as vehicles and road seeds are picked in the neighboring region moving along major axis of the objects in both directions. Table 3.1 lists empirically determined appropriate range for all the algorithm parameters. Here it is assumed that the intensity range of input image is within the range [0-1].

Parameter	Threshold Range
<i>white_th</i> (Pixel Intensity)	0.55 to 0.66
<i>min_area</i> (Pixel Count)	10 to 15
<i>max_area</i> (Pixel Count)	25 to 35
<i>diff_th</i> (Pixel Intensity)	0.16 to 0.24

Table 3.1 Range of appropriate threshold values for algorithm parameters.

3.2 Road Extraction

Detected road seeds can be used further for road extraction. Starting with detected road seeds, road extraction is carried out with the help of Fourier descriptor based road tracking algorithm developed in [18]. A local homogeneous region around a pixel enclosed by a polygon is defined as the pixel footprint and it is represented as distance function between the center pixel and pixels on the enclosing polygon. This function is then mapped to the frequency domain using discrete Fourier transform and smoothed by discarding the coefficients corresponding to higher frequencies to get normalized footprint for the pixel. The dominating peaks of the normalized footprint denote the direction along the road and tracking will be continued in that direction till entire road network is extracted. The performance of the road tracking algorithm is improved by replacing the identified vehicle pixels with appropriate road pixels from the complementary image.

3.3 Results

A pair of 0.8 meter resolution CARTOSAT-2 images acquired on December 2008 and January 2009 was used for the experiments. The sun elevation angles for images were 38.57 degrees and 37.57 degrees respectively and were of dimension 9792 x 9792 pixels. Several subsets of these images were prepared manually. The performance of the our road extraction method on these subset images is discussed in this section.

The working of the vehicle detection algorithm is demonstrated on a pair of images of size 186 x 274 shown in Fig. 3.1. Fig. 3.1(c) shows the difference between the input images. Fig. 3.1(d) and Fig. 3.1(f) shows the binary thresholded input images while Fig. 3.1(e) and Fig. 3.1(g) shows area thresholded results. Fig. 3.1(h) shows the resultant image after discarding objects with similar intensity values in both the images. Vehicle detection results are shown in Fig. 3.1(i). The algorithm is able to detect 3 vehicles including one false positive (shown enclosed in a ellipse). Road seeds are then identified in the neighborhood of detected vehicles. These road seeds are fed to road tracking algorithm. Extracted road regions are shown in Fig. 3.1(j). Because of false positives produced by the vehicle detection method, the road tracking algorithm has also labeled a small non-road region as road.

Road extraction result on a pair of images of size 523 x 2305 is shown in Fig. 3.2. The vehicle detection algorithm was able to detect five vehicles. However number of false positives was increased

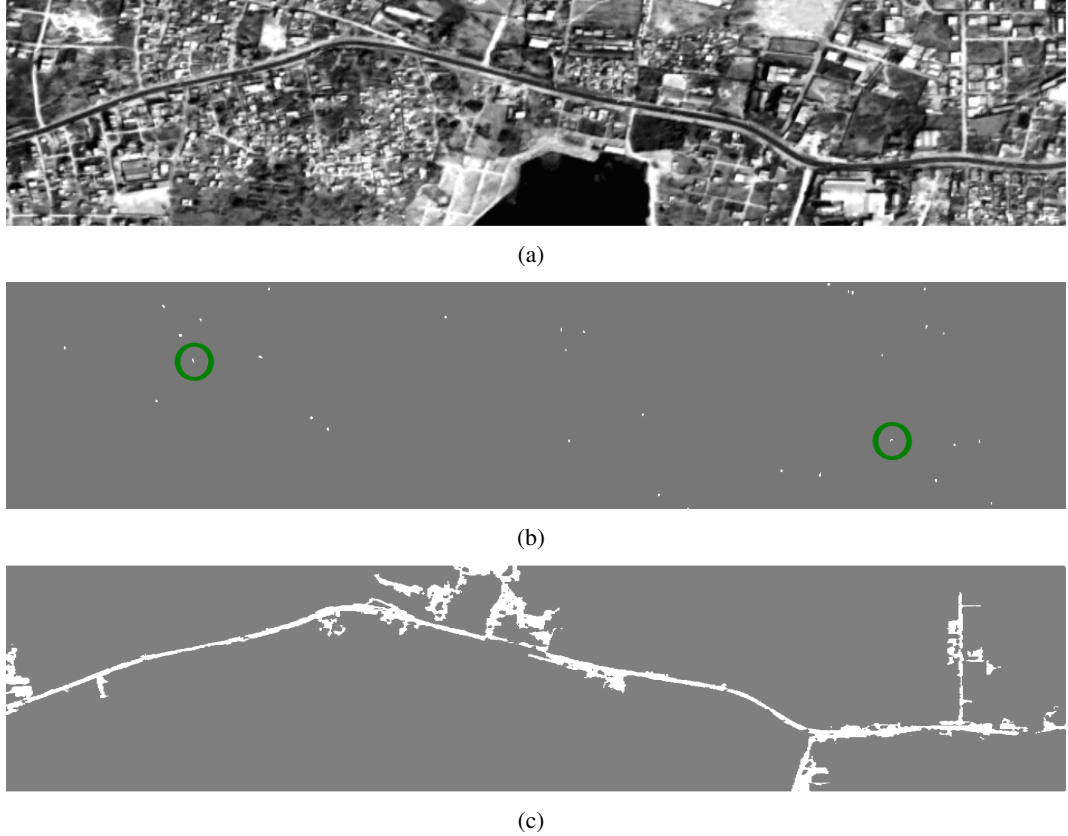


Figure 3.2 (a) CARTOSAT-2 input image, (b) vehicle detection result and (c) extracted road network. Detected vehicles are marked with circles.

considerably to 18. The road tracking algorithm was modified to discard the road seeds based on area of road region that was extracted with the aid of that particular road seed. The road extraction presented in [18] may grow out of road region and wrongly label such region as road. This limitation of the algorithm can be observed in the road extraction result in Fig. 3.2. Road extraction algorithm parameters were set according to the suggestions in [18]. Fig. 3.3 shows the road extraction results on another pair of images of size 512 x 512.

3.4 Discussion

In this chapter we have demonstrated the utility of high resolution multi-temporal images in automatic road seed extraction. Intuitively, since the road seeds are picked from areas around the detected vehicles, higher confidence about the road seeds can be assumed. This is confirmed by the experimental results. We have discussed only the extraction of bright vehicle patches in the background of dark road pixels. However, the algorithm can be modified to extract even dark patches of vehicles over rather bright background road pixels by setting appropriate values to algorithm parameters.

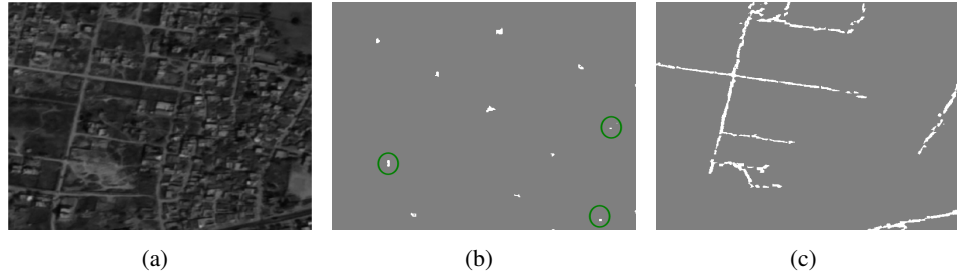


Figure 3.3 (a) CARTOSAT-2 input image, (b) vehicle detection result and (c) extracted road network. Detected vehicles are marked with circles.

Higher accuracy in road seed extraction can be obtained by using scenes with shorter time gap. However, accuracy is also dependent on georeferencing scheme adapted by satellite image providers. Both larger time gap and large geometric distortion will result in considerable increase in false positive. On the other hand, scenes with too many vehicles will result in detection of large number of road seeds which introduces further constraint on time of the day of the acquisition of the image. The other extreme, images with no vehicles, are rare since a typical satellite image covers a large geographic area (Example, for CARTOSAT-2 image minimum area of interest is 25 square kilometers).

Though road tracking algorithm in [18] has been successful in extracting road, it has also wrongly labeled significantly large non-road area as road region. Also, the algorithm requires considerably large number of road seeds [19]. In the next chapter we will introduce a new road extraction algorithm which will employ road texture features to enhance the road tracking.

Chapter 4

Adaptive Texture Matching For Road Extraction

Road model adopted in the road extraction techniques is an important factor influencing the accuracy of the road extraction results. Though several road extraction techniques have been proposed in the past, because of various assumptions about the road region characteristics and imaging modality, such techniques often exhibit limited success in the real scenarios. Hence, in this chapter we aim to develop a road extraction technique that satisfies the following:

- minimal manual intervention;
- can be applied on scenes with varying road surface characteristics (texture);
- for images of various spatial resolutions; and
- images containing road region with varying widths and curvatures.

In [4], based on road models used in different road extraction techniques, *road* is defined to be geometrically a long and continuous object with narrow width, to be radiometrically an object made of slowly varying grayscale and texture. Impact of the chosen road model on road extraction accuracy can be minimized if the road model is built based on input image characteristics and road model parameters are made to adapt to the local road region characteristics.

Based on above observations, this chapter presents a novel adaptive texture matching based road extraction algorithm, ATM-R, in which road region templates are derived from already detected road regions. The algorithm can start with automatically detected seeds (Chapter 3) or can start from user provided reference regions. We first present a general framework which enables such road template generation and template matching in terms of arbitrary texture features. The framework attempts to grow the road in the direction of lastly detected road region by observing the road texture trends in last few detected road regions. The discussion in this chapter is based on road extraction technique presented in [26].

As stated in [27], “an image region has a constant texture if a set of local properties in that region is constant, slowly varying or approximately periodic”. An excellent study of image features that can capture such local properties using various color, texture and shape image feature can be found in [28].

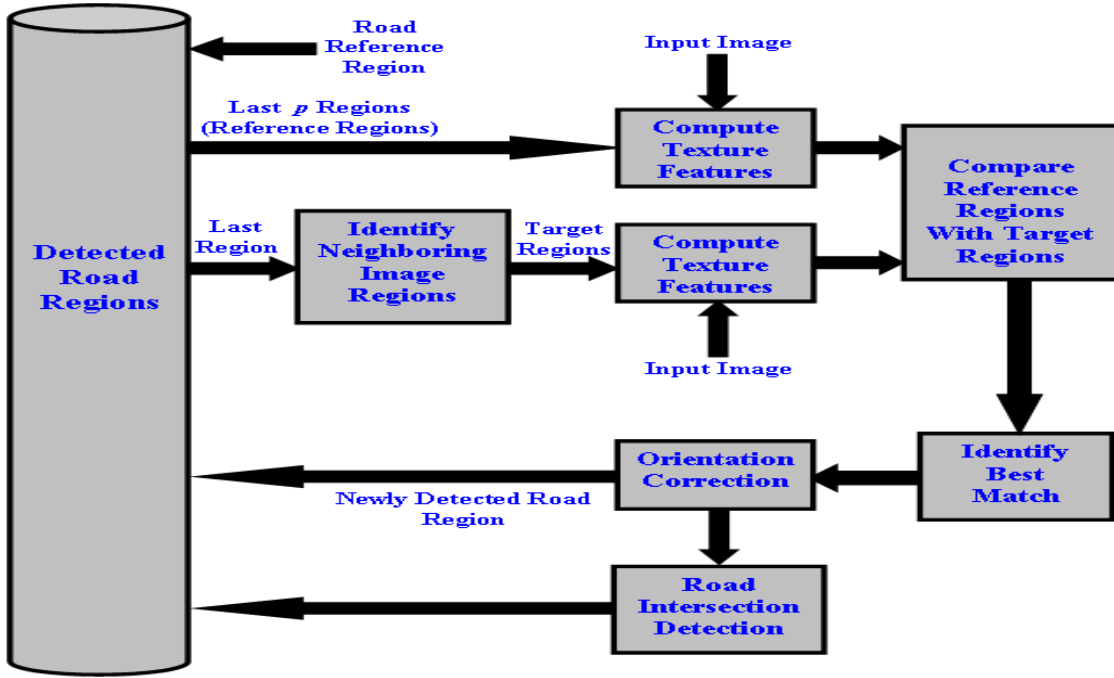


Figure 4.1 Block diagram of proposed ATM-R algorithm

In our experiments we have used Tamura features [29], k-means based features and histograms for road texture matching in our framework. A technique to find orientation of binary objects presented in [30] is used for finding the orientation of the detected road regions. Road region orientation information is further utilized in finding road intersections. This work draws its initial inspiration from profile matching technique presented in [31]. Performance of the algorithm on high resolution IKONOS, CARTOSAT-2 and Google Earth images is discussed.

4.1 Road Extraction Algorithm

This section discusses the proposed ATM-R algorithm in detail. Starting from user provided reference road region, the algorithm generates a set of target road candidate regions and searches for best candidate region based on various texture features. Detected road regions are further utilized as reference regions for subsequent comparisons. The block diagram of ATM-R algorithm is shown in Fig. 4.1.

4.1.1 Framework for Road Extraction

Consider a set of n image feature vectors

$$\mathbf{F} = [\vec{f}_1, \vec{f}_2, \dots, \vec{f}_n], \quad (4.1)$$

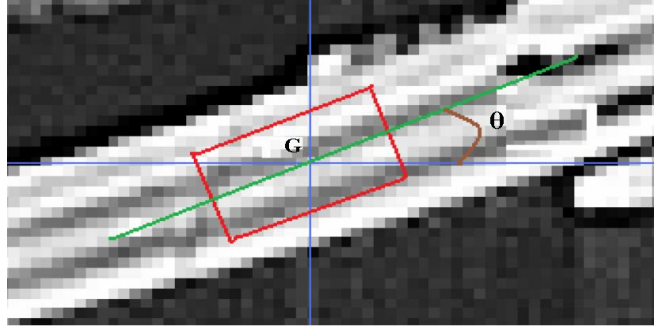


Figure 4.2 A representation of road region. Road region enclosed in rectangle is represented in terms of location G and angle θ .

a set of n respective distance functions

$$\mathbf{M} = [m_1, m_2, \dots, m_n] \quad (4.2)$$

and a set of n respective weight coefficients

$$\vec{W} = [w_1, w_2, \dots, w_n]^T. \quad (4.3)$$

\mathbf{F} is normalized such that $0 \leq f_{ij} \leq 1, \forall i \in 1, 2, \dots, k_j, \forall j \in 1, 2, \dots, n$, where k_j is the dimension of j^{th} feature vector. \vec{W} is normalized such that

$$\sum_{i=1}^n w_i = 1. \quad (4.4)$$

A rectangular road region can be represented in terms of its centroid G and its orientation θ with x -axis (along track) as shown in Fig. 4.2. Of the detected road segments, consider a set of last p adjacent rectangular road regions

$$\mathbf{R} = [r_{(g_1, \theta_1)}, r_{(g_2, \theta_2)}, \dots, r_{(g_p, \theta_p)}], \quad (4.5)$$

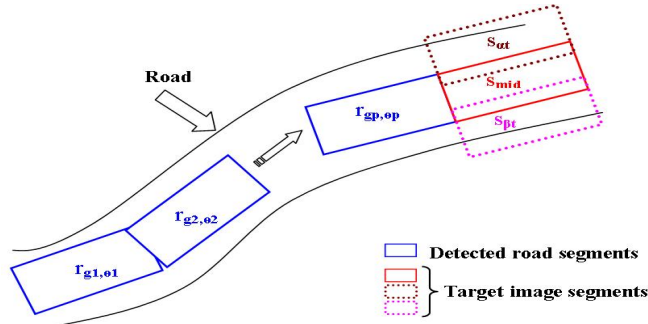


Figure 4.3 Proposed road extraction framework. Target regions s_{mid} , s_{α_t} and s_{β_t} are compared with detected road regions $r_{(g_1, \theta_1)}$ to $r_{(g_p, \theta_p)}$.

Feature	Distance Function	Weight Coefficient
Tamura features: Contrast, Directionality	Euclidean	0.3077, 0.1538
k-means based features: minimum, maximum and average intensity of road cluster	k-means based distance function	0.4615
Histogram	Histogram quadratic distance	0.0769

Table 4.1 Choice of image features, distance functions and corresponding weight coefficients

each of length l and height h ($l > h$), where $\{g_1, g_2, \dots, g_p\}$ are centroids of respective rectangular regions and $\{\theta_1, \theta_2, \dots, \theta_p\}$ are orientations of respective rectangular regions with x -axis. For each such rectangular region, feature vectors can be calculated to generate reference feature set

$$\mathbf{F}_R = [\mathbf{F}_{r_1}, \mathbf{F}_{r_2}, \dots, \mathbf{F}_{r_p}]. \quad (4.6)$$

To find the next road region, a set of $(2 * t + 1)$ target rectangular regions

$$\mathbf{S} = [s_{(g_{mid}, \theta_p)}, s_{(g_{\alpha_1}, \theta_p)}, s_{(g_{\beta_1}, \theta_p)}, s_{(g_{\alpha_2}, \theta_p)}, s_{(g_{\beta_2}, \theta_p)}, \dots, \\ s_{(g_{\alpha_t}, \theta_p)}, s_{(g_{\beta_t}, \theta_p)}] \quad (4.7)$$

are matched with \mathbf{R} . Here t is number of neighbors considered at each side, $s_{(g_{mid}, \theta_p)}$ is rectangular region obtained by traversing a distance l from $r_{(g_p, \theta_p)}$ in the orientation θ_p along the length, $\{s_{(g_{\alpha_1}, \theta_p)}, s_{(g_{\alpha_2}, \theta_p)}, \dots, s_{(g_{\alpha_t}, \theta_p)}\}$ are rectangular regions obtained by sliding $s_{(g_{mid}, \theta_p)}$ $\{1, 2, \dots, t\}$ pixels along width towards left on cross track and $\{s_{(g_{\beta_1}, \theta_p)}, s_{(g_{\beta_2}, \theta_p)}, \dots, s_{(g_{\beta_t}, \theta_p)}\}$ are rectangular regions obtained by sliding $s_{(g_{mid}, \theta_p)}$ $\{1, 2, \dots, t\}$ pixels along width towards right on cross track. This arrangement is illustrated in Fig. 4.3. For each such rectangular region, feature vectors can be calculated to generate target feature set,

$$\mathbf{F}_S = [\mathbf{F}_{s_{mid}}, \mathbf{F}_{s_{\alpha_1}}, \mathbf{F}_{s_{\beta_1}}, \mathbf{F}_{s_{\alpha_2}}, \mathbf{F}_{s_{\beta_2}}, \dots, \mathbf{F}_{s_{\alpha_t}}, \mathbf{F}_{s_{\beta_t}}]. \quad (4.8)$$

To compare a target region feature vectors \mathbf{F}_s with a reference region feature vectors \mathbf{F}_r , first, distance between each pair of features is computed using respective distance function defined in Eqn. 4.2 and a distance vector

$$\vec{D}_{rs} = [d_1, d_2, \dots, d_n]^T \quad (4.9)$$

is generated. Distance between \mathbf{F}_s and \mathbf{F}_r is then given by

$$d_{rs} = \sum_{i=1}^n d_i * w_i. \quad (4.10)$$

Since both \mathbf{F} and \vec{W} are normalized, d_{rs} will be in the range (0,1). Computed distances between \mathbf{F}_R and \mathbf{F}_S , hence, can be represented as a matrix \mathbf{D}_{RS} of dimension $p \times (2 * t + 1)$ and the target rectangular region with least distance in \mathbf{D}_{RS} is tagged as next valid road region, $r_{(g_{p+1}, \theta_p)}$. The procedure continues till it encounters a region for which all the distances in \mathbf{D}_{RS} are above a predefined threshold, $dist_th$.

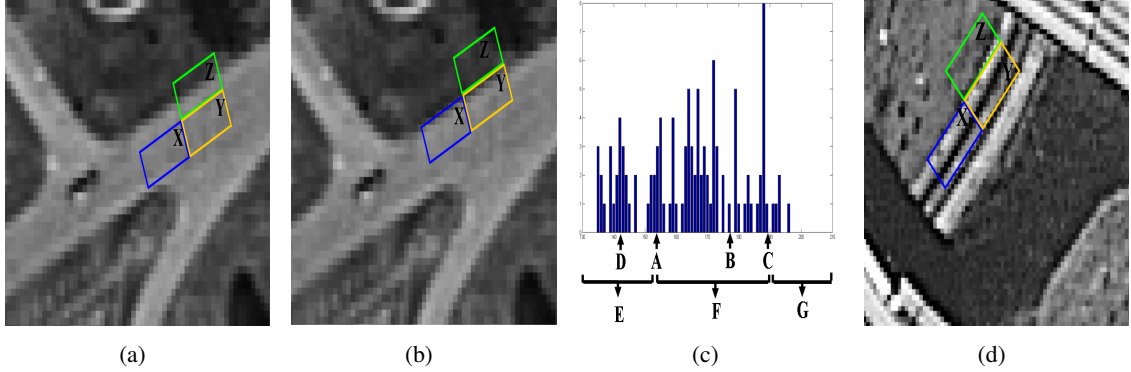


Figure 4.4 Texture features. (a) A scenario where texture feature contrast can be useful, (b) a possible scenario where contrast can produce ambiguous results, (c) scheme to choose road and non-road cluster center for a image region and (d) sample image region where road and non-road can be discriminated using directionality.

4.1.2 Choice of Image Features and Distance Functions

Table 4.1 lists the image features and respective distance function used in our experiments. Of these texture features, Tamura features [29], which capture low level statistical properties of textures, have been successfully deployed in various content based image retrieval (CBIR) systems [32] - [36]. Suitability of those features to road extraction problem and their computation is explained in the following subsections.

4.1.2.1 Contrast

Contrast signifies the intensity variation present in an image and captures the polarization between black and white regions [28]. Assuming road regions will have contrasting surrounding, in this context of road texture matching, contrast can be used to avoid growing road out of road boundaries as depicted in Fig. 4.4(a). In the figure, detected road region is labeled as X and regions labeled Y and Z are being compared with detected road region. Region labeled Y is of similar contrast to that of detected road region, whereas region Z will show significant difference in the contrast. In our experiments, contrast is computed using definition in [29]:

$$f_{contrast} = \sigma / (\alpha_4)^\gamma \quad (4.11)$$

where γ is a positive number, σ is the standard deviation of the gray-level probability distribution and α_4 is the kurtosis. The kurtosis is defined as,

$$\alpha_4 = \mu_4 / \sigma^4 \quad (4.12)$$

where μ_4 is the fourth central moment of the gray-level probability distribution. Euclidean distance is used for matching contrast of two given regions.

4.1.2.2 k-means Based Features and Distance Function

Texture matching based only on contrast is not sufficient to distinguish between homogeneous regions belonging to two different objects as illustrated in Fig. 4.4(b). In the figure, contrast of detected road region(labeled X) will be similar to that of regions labeled Y and Z. Texture features based on the intensity values of the region are required in such scenarios. In our work, in order to capture the intensity trends of road regions, k-means clustering [37], [38] is applied to each of the reference road region in \mathbf{R} (Eqn. 4.5) and each region is clustered into two classes, road and non-road. Cluster with largest area is then labeled as road and remaining area as non-road regions. Minimum, maximum and average of intensity values of pixels belonging to road region, say $r_{min}, r_{max}, r_{avg}$, are then treated as features representing entire reference road regions in \mathbf{R} . On the similar lines a target rectangular region, say s , which needs to be validated for being road segment, is clustered into two classes and average intensity value of the cluster with larger area, say s_{avg} , is computed. Then distance between \mathbf{R} and target region is computed as follows:

$$D(\mathbf{R}, s) = \begin{cases} |s_{avg} - r_{avg}| & \text{if } (r_{min} - e.th) \leq s_{avg} \leq (r_{max} + e.th) \\ 1 & \text{otherwise} \end{cases} \quad (4.13)$$

where $e.th$ is a predefined threshold which lets the target regions to have average intensity values marginally outside the observed trend in reference set. Here it is assumed that input image intensities are in the range (0,1).

Cluster Center Estimation: The k-means clustering algorithm starts with given set of cluster centers and accurate clustering of the given data set can be expected if the initial cluster centers are closer to real cluster centers. In our experiments, average of intensity values of pixels belonging to road region, r_{avg} is used as initial guess for road cluster. To compute an estimate for non-road region, first histogram of the target rectangular region (s) is computed. Intensity value, corresponding to maxima of the histogram outside the range from r_{min} to r_{max} , is treated as initial cluster center for non-road regions. For the histogram in Fig. 4.4(c), A is r_{min} , B is r_{avg} and C is r_{max} . F denotes the range of road region and E and G denote non-road region. Maxima of the non-road region is observed at D which will be considered as cluster center for non-road regions.

4.1.2.3 Histogram and Histogram Quadratic Distance

Histograms can be used to measure similarity between two image regions. In [39], quadratic-form metric, a metric to compare histograms is introduced. The quadratic form distance between histograms \mathbf{h}_1 and \mathbf{h}_2 is given by:

$$D(\mathbf{h}_1, \mathbf{h}_2) = (\mathbf{h}_1 - \mathbf{h}_2)^T \mathbf{H} (\mathbf{h}_1 - \mathbf{h}_2) \quad (4.14)$$

where \mathbf{H} , is weighing factor matrix [28]. In our experiments, each row of \mathbf{H} is generated by an array of time shifted 1D Gaussian function centered at the diagonal of \mathbf{H} . A sample matrix for histogram with 4

bins is given below:

$$\mathbf{H} = \begin{pmatrix} 1.0000 & 0.6065 & 0.1353 & 0.0111 \\ 0.6065 & 1.0000 & 0.6065 & 0.1353 \\ 0.1353 & 0.6065 & 1.0000 & 0.6065 \\ 0.0111 & 0.1353 & 0.6065 & 1.0000 \end{pmatrix}$$

4.1.2.4 Directionality

Directionality can be used to distinguish between road and non-road regions in scenarios shown in Fig. 4.4(d). Directionality of detected road region (region labeled X) is similar to that of region labeled Y but region labeled Z is significantly less directional compared to region labeled X . In our work, directionality is computed using definition in [29] and the implementation is similar to that in [40]. In [28], it is noted that directionality values are measured on the scale of 0 to 1. Euclidean distance is used for matching directionality of two given regions.

4.1.3 Orientation of Road Regions

In the process of finding the new road region $r_{(g_{p+1}, \theta_p)}$, target road regions in \mathbf{S} are divided into two clusters, road and non-road using the procedure explained in Section 4.1.2.2. Identified road cluster is further utilized to compute the corrected orientation, θ_{p+1} . In [30] the orientation of a binary object is computed by finding an ellipse that has the same normalized second central moments as the binary object. Orientation of the major axis of the ellipse with x -axis is treated as the orientation of the object. The identified road cluster is binarized and orientation is computed using method in [30].

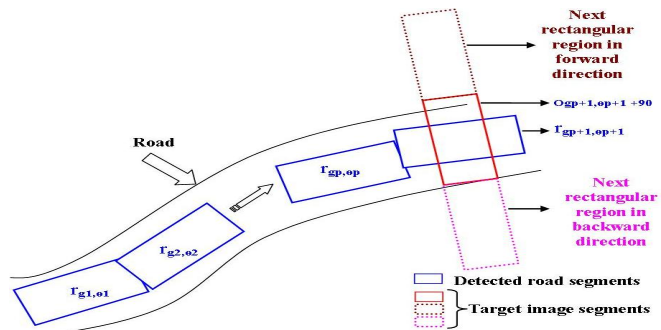


Figure 4.5 Road intersection detection. An image region $o_{(g_{p+1}, \theta_{p+1} + 90)}$ which is at 90 degree orientation with newly detected road region $r_{(g_{p+1}, \theta_{p+1})}$ will be studied for detecting road intersections.

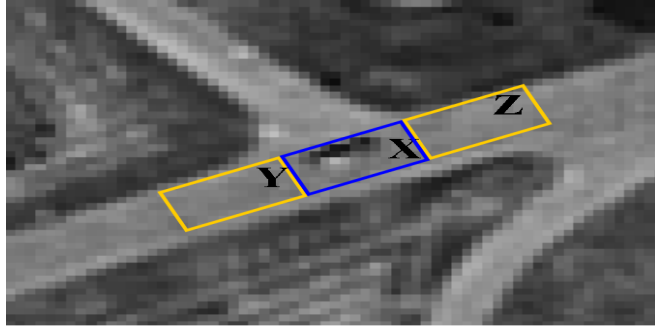


Figure 4.6 Selecting reference road region. An appropriated dimension for reference road region provided manually to the ATM-R algorithm can be assessed with the help of objects like vehicles on road that can be located in the input image, for example region labeled X.

4.1.4 Road Intersections

In order to detect the road diversions at road intersections and to track diverted roads, at each newly detected road region, $r_{(g_{p+1}, \theta_{p+1})}$, a set of oriented rectangular regions

$$\mathbf{O} = [o_{(g_{p+1}, \theta_{p+1}+45)}, o_{(g_{p+1}, \theta_{p+1}+90)}, o_{(g_{p+1}, \theta_{p+1}+135)}], \quad (4.15)$$

are matched with \mathbf{R} (Eqn. 4.5). Comparison procedure of oriented regions feature vectors

$$\mathbf{F}_O = [o_{45}, o_{90}, o_{135}] \quad (4.16)$$

with \mathbf{F}_R (Eqn. 4.6) is same as the procedure explained in Section 4.1.1. Road tracking will then continue in both the direction of all those oriented rectangular regions for which the distance is less than the threshold $dist_th$. The orientation computation explained in Section 4.1.3 can guide road extraction in any arbitrary road direction avoiding the need for exhaustive search for road diversions in all possible directions. The arrangement is illustrated for $o_{(g_{p+1}, \theta_{p+1}+90)}$ in Fig. 4.5.

Detected diverted road with length (number of detected road regions in a sequence) less than a predefined threshold, $length_th$ is discarded.

4.1.5 Initialization in case of manual seeds

Initial road region templates can be generated automatically or can be provided manually. This section gives the details of manual seed selection. During our experiments it is observed if the area of the reference road region is too small (less than 25 pixels) the road tracking can grow out of road region and label non-road region as road. On the other hand if the region is too big (more than road width) then road tracking will fail to grow in road curves and diversions. Good estimate for reference road region can be made with the help of vehicles on the road. This is demonstrated in the Fig. 4.6. The region labeled X encompasses a vehicle and is in the same orientation of the vehicle. The regions labeled Y and Z are obtained by traversing in the orientation of the vehicle in backward and forward directions

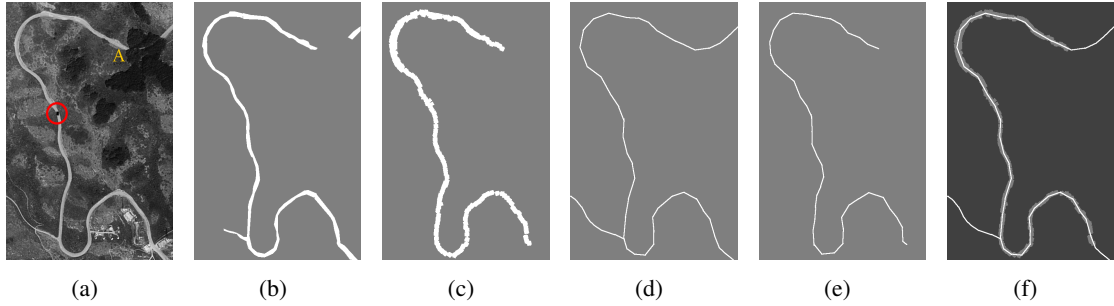


Figure 4.7 Validation of result with the help of manually created ground truth. (a) IKONOS input image, (b) road area ground truth (RAGT), (c) ATM-R extracted road area (ERA), (d) road network ground truth (RNGT), (e) ATM-R extracted road network and (f) overlay of road network ground truth on ATM-R extracted road area for validation.

respectively. These regions labeled Y and Z can further be used as reference road regions for road tracking. The orientation of the user provided road region is computed by following the procedure in Section 4.1.3. In case of scene with road regions of significantly different textures (or with disconnected road segments), multiple references representing each road texture are provided manually. In all our experiments the aspect ratio of the reference rectangular road region was approximately 1.5.

4.2 Results and Evaluation

4.2.1 Data

To assess the performance of the ATM-R algorithm, a set of images encompassing wide range of radiometric resolutions and different spatial resolutions were prepared. The images set consisted of grayscale equivalent of pan-sharpened IKONOS images, panchromatic CARTOSAT-2 images and

Image	Source	Spatial Resolution	Radio metric Res.	Image Dimension (Pixels)	Number of Reference Regions	Ref. Region Dimension (Pixels)
Figure 4.7	IKONOS	1m	11 bits	771x517	1	13x8
Figure 4.8	IKONOS	1m	11 bits	891x821	5	13x8
Figure 4.9	IKONOS	1m	11 bits	811x1036	6	11x7
Figure 4.10	IKONOS	1m	11 bits	476x995	3	13x8
Figure 4.11	IKONOS	1m	11 bits	524x498	10	10x6
Figure 4.12	CARTOSAT-2	0.8m	10 bits	460x736	2	13x8
Figure 4.13	CARTOSAT-2	0.8m	10 bits	523x2305	2	13x8
Figure 4.14	Google Earth	$\approx 1\text{m}$	8 bits	450x1048	2	13x8
Figure 4.16	Google Earth	$\approx 1\text{m}$	8 bits	650x981	1	13x8

Table 4.2 Images used in our experiments

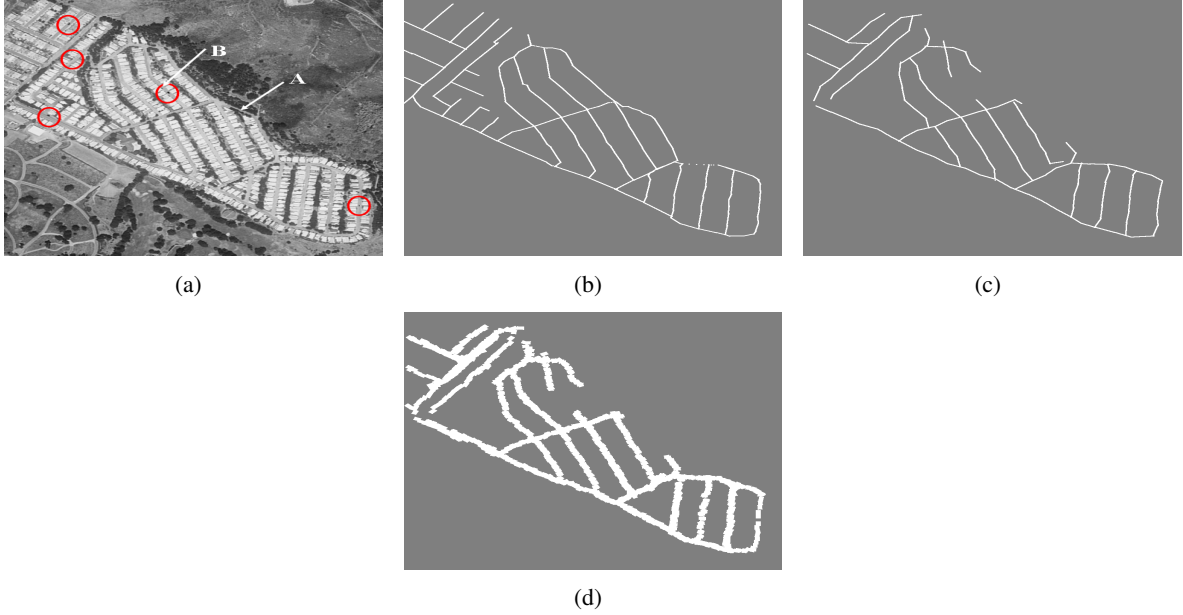


Figure 4.8 (a) IKONOS input image, (b) road network ground truth, (c) ATM-R extracted road network and (d) ATM-R extracted road area. Vegetation along the road at location labeled A and abrupt change in texture at location B has resulted in discontinuity in road network.

grayscale equivalent of images captured from Google Earth (see list in Table 4.2). Multiple subsets of IKONOS and CARTOSAT-2 images were prepared. Images were chosen to include road regions with varying width, wide range of road surface reflectance values and different textures. Experiments were conducted on images with disconnected road segments, multi-lane roads, road regions occluded with trees and images with road over-bridges.

4.2.2 Evaluation Measures

For each image used in our experiments, road area ground truth (*RAGT*) was created by manually segmenting out road regions and road network ground truth (*RNGT*) is created by joining road center line. This is shown in Fig. 4.7(b) and Fig. 4.7(d) respectively for input IKONOS image in Fig. 4.7(a). Fig. 4.7(c) and Fig. 4.7(e) are extracted road area (*ERA*) and extracted road network (obtained by joining centroids of detected adjacent road regions) for image in Fig. 4.7(a), derived using the ATM-R algorithm. The validation followed is similar to that in [41].

4.2.2.1 Road Network Completeness

RNGT is first overlaid on *ERA* (as shown in Fig. 4.7(f)) and overlap of road area pixels in a 5x5 window around each pixel of the *RNGT* is examined. Then, road network completeness, C_{net} , is calculated

Image	Predominant Road Geometry	Cnet %	Carea %	Tarea %
Figure 4.7	Narrow and curvy roads	82	75	92
Figure 4.8	Linear and parallel roads	85	75	74
Figure 4.9	Disconnected road segments	81	70	77
Figure 4.10	Varying width roads	73	68	74
Figure 4.11	Occluded road segments	80	66	83
Figure 4.12	Narrow roads	65	69	80
Figure 4.13	Wide roads with good surround contrast	96	85	84
Figure 4.14	Linear road region with poor surround contrast	92	69	66
Figure 4.16	Linear road region with poor surround contrast	97	87	75

Table 4.3 Performance of proposed algorithm

as follows:

$$C_{net} = \frac{N_{overlap}}{N_{total}} * 100, \quad (4.17)$$

where $N_{overlap}$ is number of pixels of $RNGT$ for which overlap is found and N_{total} is total number of pixels in $RNGT$.

4.2.2.2 Road Area Completeness

ERA is overlaid on $RAGT$ and road area completeness, C_{area} , is calculated as follows:

$$C_{area} = \frac{A_{overlap}}{A_{total}} * 100, \quad (4.18)$$

where $A_{overlap}$ is number of pixels of $RAGT$ for which overlap found in ERA and A_{total} is total number of pixels in $RAGT$. Both C_{net} and C_{area} measure the accuracy of road extraction result with respect to ground truth.

4.2.2.3 Correctness of ERA

The truthness or correctness of ERA , T_{area} , is calculated as follows:

$$T_{area} = \frac{EA_{overlap}}{EA_{total}} * 100, \quad (4.19)$$

where $EA_{overlap}$ is number of pixels which are accurately labeled as road pixels in ERA and EA_{total} is total number of pixels in ERA . T_{area} is a measure of the performance of the algorithm.

Performance of the ATM-R algorithm in terms of these validation indices is summarized in Table 4.3 for all the different input images used in our experiments.

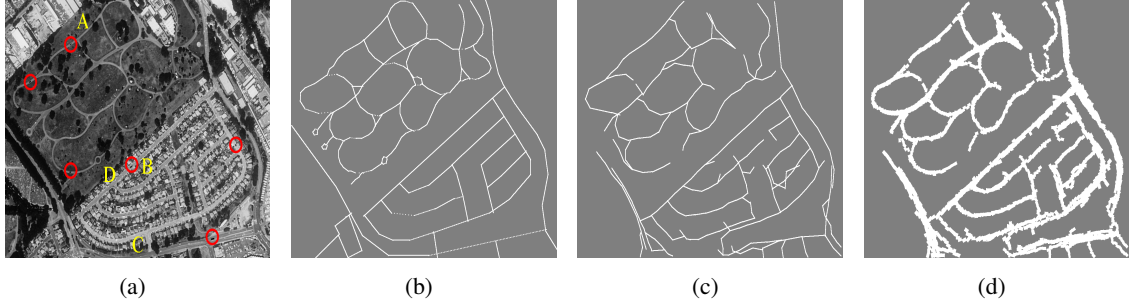


Figure 4.9 (a) IKONOS input image, (b) road network ground truth, (c) ATM-R extracted road network and (d) ATM-R extracted road area. Separate seed points were provided to extract entire road network consisting of significantly different textures (labeled *A*, *B* and *C*)

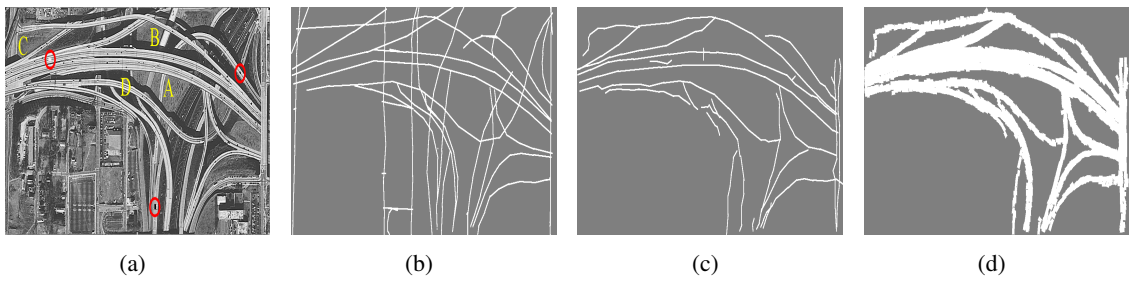


Figure 4.10 (a) IKONOS input image, (b) road network ground truth, (c) ATM-R extracted road network and (d) ATM-R extracted road area. More than 70% of the road network is extracted with the help of three road reference regions.

4.2.3 Results and Discussion

For the input image in Fig. 4.7 the ATM-R algorithm is able to extract 82% of the road network with the help of one input road reference region (marked with circle). The road extraction, however, was halted due to change in texture at location labeled *A* along the road. Each figure from Fig. 4.8 to Fig. 4.16 (except Fig. 4.15) has four sub-figures, input image (labeled a), *RNGT* (labeled b), extracted road network (labeled c) and *ERA* (labeled d). Manually provided road reference regions are marked with circles. For the input image in Fig. 4.8, 85% of the road network was extracted starting from 5 reference regions. The road network is broken at location labeled *A* because of the vegetation along the road. At location labeled *B* road tracking stopped because of the change in road intensity values which is higher than the threshold, *e_th* (see Section 4.1.2.2). Six road references were used for image in Fig. 4.9 to extract 81% of road network. The road network in this image consisted of three distinct road textures (labeled *A*, *B* and *C*). Road sub-networks tagged *A* and *B* are disconnected and at location where *B* and *C* merge (location of label *C*) a sharp transition in texture is observed. Hence at least three road reference regions are required to cover the entire network. While tracking road diversion starting at location *D*, the road grows marginally outside the road because of adjacent building sharing similar intensity values as road. Since, length of extracted diverted road segment is more than *length_th* (see

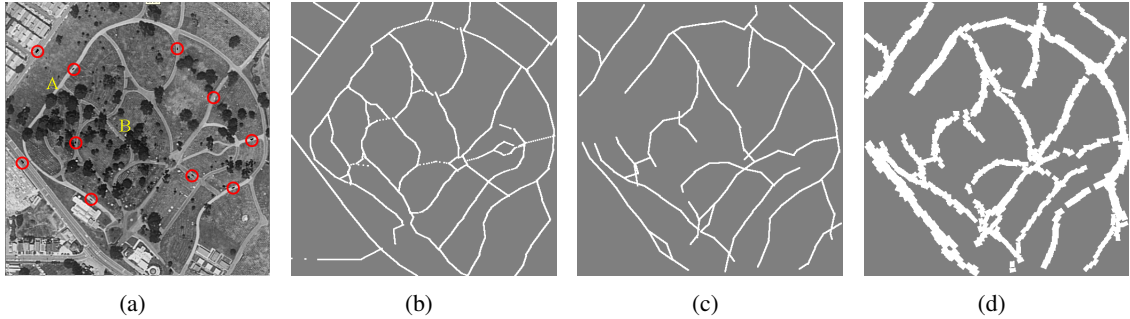


Figure 4.11 (a) IKONOS input image, (b) road network ground truth, (c) ATM-R extracted road network and (d) ATM-R extracted road area. Large amount of vegetation along the road has disrupted road extraction and as high as ten road reference region were required to extract road network.

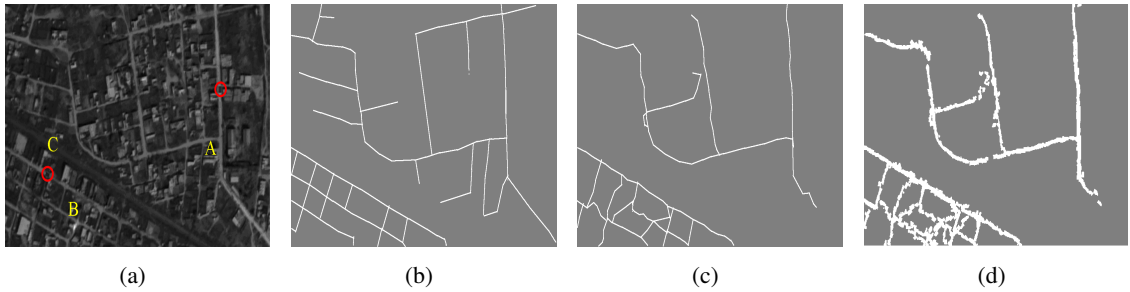


Figure 4.12 (a) CARTOSAT-2 input image, (b) road network ground truth, (c) ATM-R extracted road network and (d) ATM-R extracted road area. Proposed algorithm, being independent of image type, is able to extract road network from a CARTOSAT-2 image.

Section 4.1.4) algorithm wrongly assumes it to be a valid road region. For image in Fig. 4.10 extracted road network completeness is 73% with the help of 3 reference regions. Reduction in completeness is due to large number of small road segments (example: regions labeled *A* and *B*) most of which are discarded because of their length. Assertion that the algorithm is capable of tracking road intersections of any arbitrary orientation is verified with this image (example: road diversions at locations labeled *C* and *D*). In the input image in Fig. 4.11 road region is occluded by vegetation at several locations (example: regions labeled *A* and *B*). As a result, as many as 10 reference regions were required to extract 80% of the road network. Clearly, the texture matching is not suitable in these scenarios.

Since the reference road regions are derived from input images the ATM-R algorithm can be applied to images from different sensors. For the CARTOSAT-2 image in Fig. 4.12 the algorithm is able to extract 65% of road network with the help of two road reference regions. The image consists of two road network segments, labeled *A* and *B*, separated by a railway line labeled *C*. The algorithm is not able to extract narrow road segments (for example at location of label *A*) resulting in low extraction accuracy. In contrast, the algorithm could extract almost the entire wide road region for another CARTOSAT-2 image in Fig. 4.13.

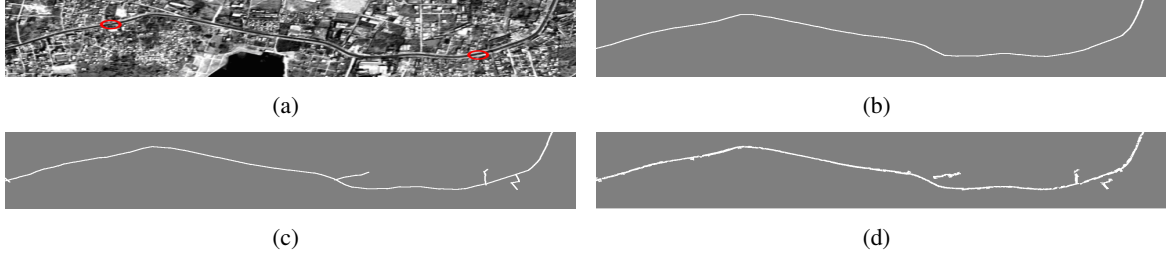


Figure 4.13 (a) CARTOSAT-2 input image, (b) road network ground truth, (c) ATM-R extracted road network and (d) ATM-R extracted road area. Entire road network is extracted with two input road reference regions.

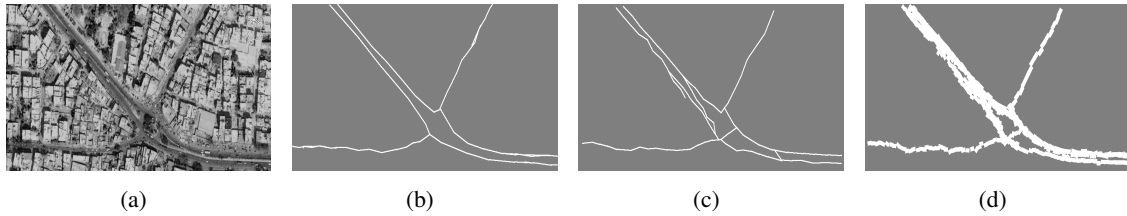


Figure 4.14 (a) Google Earth input image, (b) road network ground truth, (c) ATM-R extracted road network and (d) ATM-R extracted road area. The proposed algorithm is able to extract more than 90% of the road network.

For Google Earth images in Fig. 4.14 and Fig. 4.16 the algorithm is able to extract more than 90% of the road network. However, in our experiments we have observed that for Google Earth images road extraction often grows out of road region because of poor contrast of road region with its surroundings. This observation can also be attributed to the fact that input grayscale images were prepared from PAN sharpened Google Earth images resulting in poor quality images.

Because of mismatch between *RAGT* and *ERA* at the road edges, for most images value of C_{area} is less than C_{net} . Also, the correctness of *ERA* (T_{area}) is less for the images for which the road extraction has grown outside of road region (for example Fig. 4.9). In all our experiments *dist_th* (see

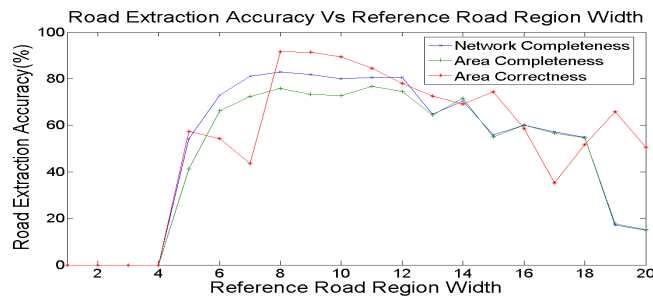


Figure 4.15 Road extraction accuracies for various widths of reference road region. Higher accuracy is observed for reference region width of 7 pixels to 13 pixels.

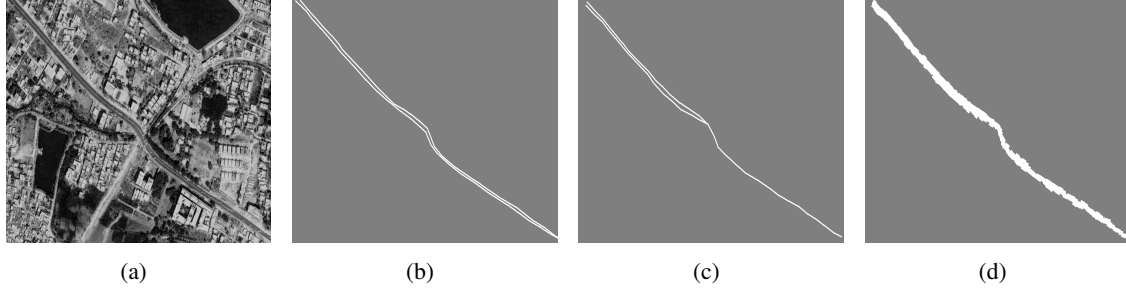


Figure 4.16 (a) Google Earth input image, (b) road network ground truth, (c) ATM-R extracted road network and (d) ATM-R extracted road area. Entire road network has been extracted by the proposed algorithm.

Section 4.1.1) was set to 0.5 and e_th (see Section 4.1.2.2) is set to 5. Empirically determined weight coefficients listed in Table 4.1 were used in all our experiments.

To understand the impact of dimension of the reference road region on algorithm performance, road extraction is carried out on input image in Fig. 4.7 for various reference region dimensions. Width of the road reference region is varied from 4 pixels to 20 pixels which is proportional to actual road width in the image. The observed performance is presented in Fig. 4.15. From the figure it can be noted that higher road extraction accuracy is obtained for widths more than 7 pixels and less than 13 pixels. This also accounts for lower extraction accuracy for input images with narrow road regions (Example Fig. 4.12).

Performance of the ATM-R road extraction algorithm is compared with road extraction algorithm in [18]. In our implementation of [18] seeds were provided manually until road extraction accuracy similar to the ATM-R algorithm or better is achieved in terms of C_{net} . Comparison of the number of seeds used in both the algorithm is listed in Table 4.4 along with observed C_{area} and T_{area} for both the algorithms. For most of the images the ATM-R algorithm has succeeded in extracting road with fewer inputs. Lower values of T_{area} for algorithm in [18] highlights the fact that the algorithm in [18] produces

Image	C_{net} %	Seeds Req. For ATM-R	Seeds Req. For Hu et al Algo.	C_{area} % For ATM-R	C_{area} % For Hu et al	T_{area} % For ATM-R	T_{area} % For Hu et al
Figure 4.7	82	1	1	75	88	92	85
Figure 4.8	85	5	9	75	74	74	42
Figure 4.9	81	6	16	70	68	77	64
Figure 4.10	73	3	32	68	55	74	87
Figure 4.14	92	2	5	69	72	66	35

Table 4.4 Comparison of performance of proposed algorithm with Fourier descriptor based road extraction algorithm

large amount of false positive road regions. However, the ATM-R algorithm is computationally more expensive than algorithm in [18].

4.3 Discussion

Tamura features, when used as global texture descriptors, have shown limited success in discriminating between different objects [28]. However, in this chapter we have demonstrated that these features can still be effective if they are used for comparing small image regions. Also, proposed algorithm significantly simplifies road intersection detection. We have demonstrated that ATM-R algorithm is capable of accurately extract road network from high resolution satellite images independent of its radiometric characteristics. The algorithm not only extracted road regions of different widths but also traced road curves and diversions of different orientations. Along with creating road network map for input images, our algorithm is able to generate valuable additional information like road area map. An accuracy of more than 70% in road extraction results, demonstrates the robustness of the ATM-R algorithm.

The ATM-R algorithm has shown better performance as compared to road extraction technique in [18] which we used in previous chapter to extract road. In the next chapter we develop a complete road extraction system which makes use automatic road seed extraction of previous chapter and road extraction technique introduced in this chapter.

Chapter 5

Road Extraction System

Road network generated from a road extraction system can be used as an input to a geographical information system for cartographic or other purposes. Maps generated from such systems are essential for navigational aids like car navigation which are needed by tourists, passenger vehicles, logistics providers and others. Of the two broad categories of road extraction systems, semi-automatic and automatic, the former requires that the user specify some initial conditions usually in the form of seed points entered manually by a human operator through some graphical user interface [17]. On the other hand, the fully automatic road extraction system is expected to work on its own. In chapter 3 we have introduced a seed extraction method using multi-temporal images and in chapter 4 we have formulated a texture matching based road tracking method (ATM-R). An obvious combination of these two methods, a fully automatic road extraction system, is presented in this chapter. Also, other potential applications of multi-temporal images which are discussed in [42] are elaborated in this chapter.

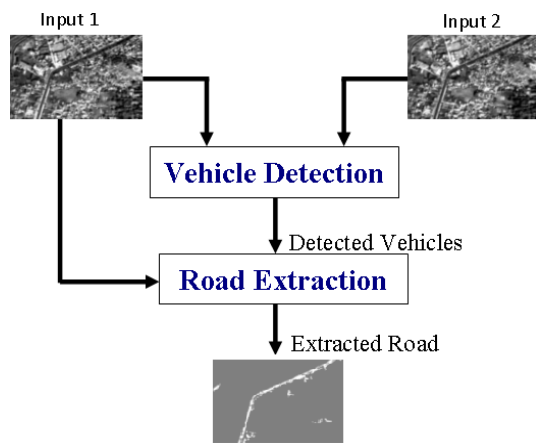


Figure 5.1 Road Extraction System Block Diagram.

Algorithm 5.1 Detect vehicles

Require: Given a pair of panchromatic images of same geographic area $x1$ and $x2$ and parameters $white_th$, min_area , max_area , $diff_th$. Detect vehicles.

Ensure:

```
 $x1\_t \leftarrow$  Threshold  $x1$  such that all the pixels in  $x1$  with gray value less than  $white\_th$  are zero.  
 $x2\_t \leftarrow$  Threshold  $x2$  such that all the pixels in  $x2$  with gray value less than  $white\_th$  are zero.  
for each 8-connected objects in  $x1\_t$  do  
    if area of the object less than  $min\_area$  or greater than  $max\_area$  then  
        Make intensity values of all pixels of the object equal to zero in  $x1\_t$ .  
    end if  
end for  
for each 8-connected objects in  $x2\_t$  do  
    if area of the object less than  $min\_area$  or greater than  $max\_area$  then  
        Make intensity values of all pixels of the object equal to zero in  $x2\_t$ .  
    end if  
end for  
for each remaining 8-connected objects in  $x1\_t$  do  
     $obj\_a \leftarrow$  average of absolute difference of intensity values of  $x1$  and  $x2$  at the location of the  
    object.  
    if  $obj\_a \leq diff\_th$  then  
        Make intensity values of all pixels of the object equal to zero in  $x1\_t$ .  
    end if  
end for  
for each remaining 8-connected objects in  $x1\_t$  do  
    if a non-zero value present in  $x2\_t$  for any pixel of the object then  
        Make intensity values of all pixels of the object equal to zero in  $x1\_t$ .  
    end if  
end for
```

Label remaining objects in $x1_t$ as individual vehicles.

5.1 System Block Diagram

Block diagram of our road extraction system is shown in Fig. 5.1. A pair of high resolution images of geographic area captured on different dates is fed to vehicle detection subsystem. Detected vehicles are marked with ellipse in the resultant image. The road extraction subsystem picks reference road region in the neighborhood of the detected vehicles and traces the road along those vehicles. The vehicle detection is detailed in Algorithm 5.1 and road extraction subsystem is explained in Algorithm 5.2. In chapter 3 we have observed that our vehicle detection method produces considerable number of false positives which further reduces the accuracy of overall road extraction. Algorithm 5.2 addresses this issue by introducing road pruning with the help of a predefined threshold $length_th$.

Algorithm 5.2 Extract road (ATM-R Algorithm)

Require: Given a panchromatic image, vehicle detection result and parameters $dist_th$, $length_th$.
Extract road region. Here x is input image and veh is vehicle detection result.

Ensure:

$R \Leftarrow$ empty set of road reference regions.

for each 8-connected object in veh **do**

- $g \Leftarrow$ centroid; $o \Leftarrow$ orientation; $l \Leftarrow$ major axis length; $h \Leftarrow$ minor axis length of the object.
- Modify major axis length and minor axis length to achieve aspect ratio of 1.5.
- Identify reference road region r in x by traversing a distance l from g .
- L : Remove the first entry in R and insert r at the end.
- Cluster r into road and non-road regions and consider orientation of road region as actual orientation of the road region r .
- Identify target road regions T by traversing a distance l from centroid of r and sliding toward left and right of it.

for each target region in T **do**

- Find distance between reference regions in R and store in D .

end for

if least distance in $D \leq dist_th$ **then**

- Label the target region corresponding to the least distance in D as road region r .
- Go to L .

else

if number of newly detected region $\geq length_th$ **then**

- Store newly detected road regions in road map.
- for** each newly detected road region **do**

 - Consider a region at an orientation of 90 degree with newly detected road region as valid road region r .
 - Go to L .

end for

end if

end if

end for

5.2 Results

The CARTOSAT-2 image pair used in experiments in Chapter 3 is again used here for studying our road extraction system. For the input image in Fig. 5.2(a) and Fig. 5.2(b) the vehicle detection result is shown in Fig. 5.2(c). One of the rightly detected vehicle marked with ellipse is further used for extracting road. Along with vehicles, the algorithm is generating large number of false detections. The final road extraction result is shown in Fig. 5.2(d). The road extraction system has successfully extracted entire road region. The system is also successful in eliminating most of the false detection at vehicle detection stage since length of road regions extracted from such road reference region was less than a predefined threshold $length_th$. Wrongly detected road region is marked with rhombus in Fig. 5.2(d).

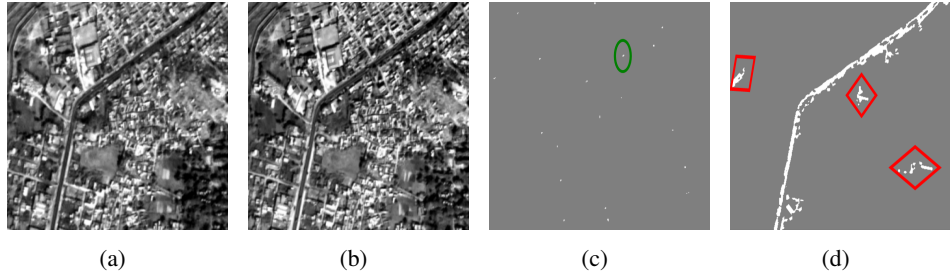


Figure 5.2 (a) CARTOSAT-2 input image, (b) second input image, (c) vehicle detection result and (c) extracted road network. Entire road network is extracted with the help of one automatic seed point marked with ellipse.

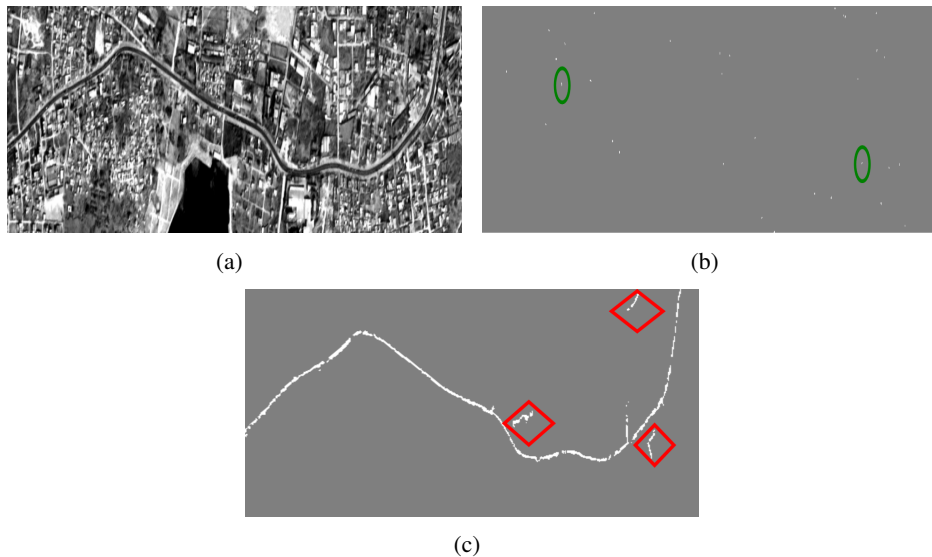


Figure 5.3 (a) CARTOSAT-2 input image, (b) vehicle detection result and (c) extracted road network. Entire road network is extracted with the help of two automatic seed point marked with ellipse.

For another image in Fig. 5.3, vehicle detection result and road extraction result is shown in Fig. 5.3(b) and in Fig. 5.3(c) respectively. Entire road network was extracted with the help of two rightly detected vehicles (marked with ellipse) with a negligible error. Wrongly detected road region is marked with rhombus in Fig. 5.3(c).

5.3 Other Potential Applications of Multi-temporal Images

5.3.1 Rail Network Extraction

Along with vehicles on the road, difference of multi-temporal images can provide clue for presence of trains on the railway network. With appropriate modification, the vehicle detection algorithm in [25]

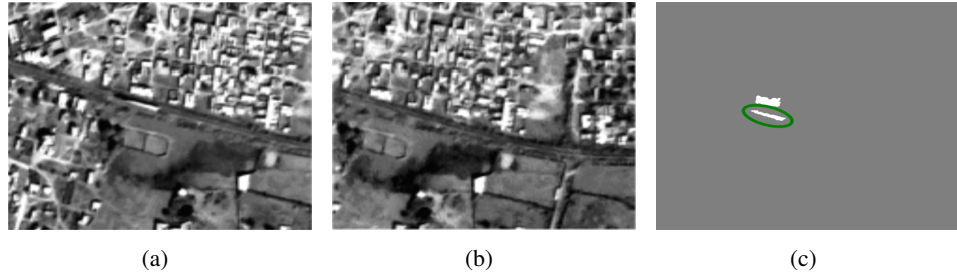


Figure 5.4 Train detection result. First two figures are input images and third one shows detected train marked with ellipse.

can easily be extended to detect such trains. The Fig. 5.4 shows detection of a train on rail network by modifying area thresholds of vehicle detection algorithm. Detected trains can further be used for extracting rail network. This provides an important way to produce georeferenced map of the entire rail network with considerable accuracy. This is particularly significant when rail network is large like that of Indian Railways and superior to approaches like the GPS based approach which demands considerable time and manpower for data collection and updating the GIS databases.

5.3.2 Defense Applications

Survey and mapping of the locations of self and enemy's physical infrastructure is essential in defense applications. Also many strategic planning aspects require to closely monitor changes in these formations and objects, especially in the sensitive regions like international boundaries. Process of studying small changes in pair of high resolution satellite imagery introduced in Chapter 3 can be extended to monitor the formation of temporary built up areas, like military structures with minimal manual inputs. The information derived from such studies can be useful in strategic planning and decision making.

5.3.3 Monitoring Large Infrastructure

With the rapid economic development of a country, infrastructure development also takes place. In India, importance is given to the Golden Quadrilateral project and other similar large road projects. Such projects of national importance demand for regular monitoring of the progress and assessment of the outcome. Given the large spatial spread of these works and the time periods of such work execution, remote sensing can play a major role in such monitoring exercises. The changes detected in multi-temporal images can be effectively utilized for monitoring the progress of such construction, by detecting the newly constructed road regions. Also, it will further help in updating the existing road databases on a regular basis. Another possibility is to detect the surface roughness of these roads which can aid in understanding the quality of the road surface.

5.3.4 Extracting Large Water Bodies

A study of multi-temporal images of a geographic region with large water bodies can lead to detection of ships and boats. Detected ships can be used as seeds to extract navigable channels like rivers. Detection of ships can also lead to extraction of large water bodies like sea. Unlike vehicles and trains, in case of ships we can expect non-ambiguous contrasting background (of water). Hence, change study using a pair of high resolution multi-spectral images can produce reliable ship detection and labeling that can have further applications in monitoring of such objects in the coastal regions and can improve the decision making at some of the man-made ports.

5.4 Discussion

We have demonstrated a fully automatic road extraction system in this chapter. Utility of multi-temporal images for various other applications like train detection, ship detection which can be further used for respective transport network extraction is also discussed. An important feature of this approach of detecting and mapping longitudinal features along with its width characteristics is that expensive field ground truth data generation can be avoided and the visual examination of the images can be used to validate the outcome thus improving the overall system performance.

Chapter 6

Conclusions

There exists a useful relationship between locations where a typical road tracking method based on region growing fails (shadow, vehicles) and the locations of extrema in the difference of closely dated images of the same geographic area. Hence, by analyzing the small change in closely dated images a valuable prior information about possible locations where road tracking may fail can be generated. This prior information will create a platform for introducing high level information about road characteristics (example, bypass vehicles and shadows on the road) more reliably into the road model. In this thesis, we have demonstrated this idea with the help of a vehicle detection algorithm (chapter 3) which addressed following challenges: (a) Variation in reflectance values of a same geographical location across the images due to difference in sun elevation angle. (b) Variation in shadow of large objects due to difference in sun elevation angle. (c) Variation in reflectance values due to misalignment between two images (because of geometric distortion) (d) Presence of non-stationary objects other than vehicles. Extension of the vehicle detection algorithm to detect train gives insight about the information content in the difference image of a pair of multi-temporal images taken at two closely dated satellite revisits.

In order to develop road extraction technique independent of spectral and spatial resolution of the input image the road templates and other road model parameter need to be derived from same input image. Hence, we have developed a framework where road texture can be analyzed and compared in terms of arbitrary texture descriptors (chapter 4). Along with utilizing various texture descriptors present in the literature we have experimented a simple k-means based descriptors in our road extraction framework. We have addressed the issues in combining our road seed extraction algorithm with our road extraction algorithm (chapter 5) and we have successfully demonstrated the working of fully automatic road extraction system.

Performance of the proposed road extraction algorithm has been assessed based on road extraction results obtained on a set of images consisting of grayscale equivalent of pan-sharpened IKONOS images, panchromatic (grayscale) CARTOSAT-2 images and grayscale equivalent of images captured from Google Earth. Images were chosen to include road regions with varying width, wide range of road surface reflectance values and different textures. Experiments were conducted on images with disconnected road segments, multi-lane roads, road regions occluded with trees and images with road over-bridges.

The measures used to evaluate the algorithm performance are road network completeness, road area completeness and correctness of road area. The algorithm is able to consistently extract 70% to 90% of the road network and has a high performance against all the three measures which demonstrates the robustness of the proposed road extraction system.

We have also discussed the limitations of the proposed road extraction system. Our road seed extraction algorithm generates considerable amount of false positives because of misalignment in input image pair due to geometric distortion. Incorporating sun angle correction can improve accuracy of road seed detection. Also, our road extraction algorithm has shown limited success in scenarios with road regions with large occlusions. Higher accuracy in road extraction can be achieved by incorporating road characteristics prior into our road extraction framework. Also, our road extraction framework gives scope to experiment with various other texture descriptors to represent road texture. Future work can also focus on estimating other additional useful road characteristics like road width along with extracting road network. Finally, change study focusing on small changes in a pair of high resolution satellite images can be extended to various other applications beyond road extraction. We have speculated about different applications of multi-temporal images including defense applications in chapter 5.

Appendix A

Image Specifications

Images used in this research consisted of grayscale equivalent of pan-sharpened IKONOS images, panchromatic CARTOSAT-2 images and grayscale equivalent of images captured from Google Earth. This appendix discusses the image specifications of these satellite images. Image specifications for CARTOSAT-2 and IKONOS images are summarized in Table A.1.

A.1 CARTOSAT-2

CARTOSAT-2 is an Earth observation satellite in a sun-synchronous orbit. The satellite is built, launched and maintained by the Indian Space Research Organization (ISRO). CARTOSAT-2 carries a state-of-the-art panchromatic camera that take grayscale pictures of the earth in the visible region of the electromagnetic spectrum. The swath covered by these high resolution PAN cameras is 9.6 kilometers and their spatial resolution is upto 0.8 meters. The satellite can be steered up to 45 degrees along track and 26 degrees across the track.

A.2 IKONOS

IKONOS is a commercial earth observation satellite and offers multispectral and panchromatic imagery. IKONOS is a 3-axis stabilized spacecraft known as the LM900 satellite bus system. Its capabilities include capturing a 3.2 meters multi-spectral, Near-Infrared (NIR) 0.82 meters panchromatic resolution at nadir. The IKONOS Satellite sensor can be programmed to acquire Stereo IKONOS Satellite Image data for the production of Digital Surface Models (DSM's) or Digital Elevation Models (DEM's) with postings of less or equal to 5 meters. From the Stereo pair the near nadir scene will be utilized to produce less than one meter Natural Color Satellite Image mosaic.

SATELLITE		
SPECIFICATIONS	CARTOSAT-2	IKONOS
Orbit	Sun synchronous	Sun synchronous
Altitude	630.6 kilometers	681 kilometers
Inclination	97.914 degrees	98.1 degrees
Swath	9.6 km	11 km
Revolutions around the earth	14.78 per day	14.7 per day
Revisit	4 to 5 days	3 days
Repetivity	310 days	144 days
Spatial resolution at nadir	0.8 meters panchromatic	0.82 meters panchromatic, 3.2 meters multi-spectral
Image bands	Panchromatic	Panchromatic, blue, green, red, near IR
Radiometric resolution	10 bits	11 bits

Table A.1 Image Specifications

A.3 Google Earth

Google Earth is a virtual globe, map and geographic information program. It maps the Earth by the superimposition of images obtained from satellite imagery, aerial photography and GIS 3D globe. Google Earth displays satellite images of varying resolution of the Earth's surface with most land is covered in at least 15 meters of resolution. The highest resolution image that can be obtained from Google Earth is at 15 cm. Images used in our experiments were from Digital Globe sourced through Google Earth and images were of approximately one meter spatial resolution with radiometric resolution of 8 bits.

Related Publications

- [1] Vinay Pandit and K.S.Rajan, “Adaptive texture matching for road extraction”, Submitted for peer review to IEEE Transactions on Image Processing.
- [2] Vinay Pandit and K.S.Rajan, “Potential applications of high resolution multi-temporal imageries”, ISRS Symposium 2009.
- [3] Vinay Pandit, Sudhir Gupta and K. S. Rajan, “Automatic road network extraction using high resolution multi-temporal satellite images”, Proceedings of IEEE IGARSS 2009.
- [4] Vinay Pandit, Sudhir Gupta and K. S. Rajan, “Color based urban scene classification using high resolution satellite Imagery”. Accepted for IPCV-2009 (not presented).

Bibliography

- [1] Q. Zhang and I. Couloigner, “An integrated approach to extracting urban road networks from high resolution multi-spectral imagery”, 1st EARSeL Workshop of the SIG Urban Remote Sensing, Berlin, 2006.
- [2] R. Peteri, J. Celle and T. Ranchin, “Detection and Extraction of Road Networks from High Resolution Satellite Images”, Proceedings of International Conference on Image Processing 2003, V1, pp.301-304.
- [3] D. Xiong, “Automated Road Network Extraction from High Resolution Images”, National Consortia on Remote Sensing in Transportation, Technical Notes, Issue 3, May 2001.
- [4] J. Park, R. Saleh and Y. Yeu, “Comprehensive Survey of Extraction Techniques of Linear Features from Remote Sensing Imagery for Updating Road Spatial Databases”, ASPRS-ACSM Annual Conference and FIG XXII Congress, 2002.
- [5] R. Bajcsy and M. Tavakoli, “Computer recognition of roads from satellite pictures,” IEEE Trans. Syst., Man, Cybern., vol. SMC-6, no. 9, pp. 623637, Sep. 1976.
- [6] P. Aluir, M. Giovane and R. Zanin, “Automatic extraction of road seeds from high-resolution aerial images”, Anais da Academia Brasileira de Ciencias, pp. 509-520, 2005.
- [7] J. Mena, “State of the art on automatic road extraction for GIS update: a novel classification”, Pattern Recogn. Lett., vol. 24, no. 16, pp. 3037-3058, December 2003.
- [8] M. Ziou, C. Armenakis and S. Wang, “Survey of work on road extraction in aerial and satellite images”, Universite de Sherbrooke, Technical report, 2000.
- [9] S. Udomhunsakul, “Semi-automatic road detection from satellite imagery”, Proceedings of ICIP 2004, pp. 1723 - 1726.
- [10] D. Ballard and C. Brown, Computer vision, Prentice-Hall, 1982, pp 131-137.
- [11] J. Cheng-Li, J. Ke-Feng, J. Yong-Mei and K. Gang-Yao, “Road extraction from high-resolution SAR imagery using Hough transform”, Proceedings of IGARSS 2005, pp. 336 - 339.

- [12] J. Cheng-Li, K. Gangyao, Y. Wenxian, "An Improved Method of Speckle Filtering in SAR Image based on Structure Detection", CIEEE International Conference on Robotics, Intelligent Systems and Signal Processing, 2003. 10.
- [13] Y. Xiao, T. Tan and S. Tay, "Utilizing edge to extract roads in high-resolution satellite imagery", Proceedings of ICIP 2005, pp. 637-640.
- [14] Y. Chen, Y. Gu, J. Gu, J. Yang, "Particle filter based road detection in SAR image", IEEE International Symposium on MAPE 2005, pp. 301 - 305.
- [15] M. Amo, F. Martinez and M. Torre, "Road extraction from aerial images using a region competition algorithm," IEEE Trans. Image Process., vol. 15, no. 5, pp. 1192-1201, May 2006.
- [16] S. Zhu and A. Yuille, "Region competition: Unifying snakes, region growing, and Bayes/MDL for multiband image segmentation," IEEE Trans. Pattern Anal. Mach. Intell., vol. 18, no. 5, pp. 884-900, May 1996.
- [17] O. Tuncer, "Fully Automatic Road Network Extraction from Satellite Images", 3rd International Conference on Recent Advances in Space Technologies, pp. 708-714, 2007.
- [18] J. Hu, A. Razdan, J. Femiani, P. Wonka and M. Cui, "Fourier shape descriptors of pixel footprints for road extraction from satellite images", Proceedings of ICIP 2007, pp. 49-52.
- [19] J. Hu, A. Razdan, J. Femiani, M. Cui and P. Wonka, "Road Network Extraction and Intersection Detection From Aerial Images by Tracking Road Footprints", IEEE Transaction on geosciences and remote sensing, Vol. 45, No. 12, 2007, pp. 4144 - 4157.
- [20] E. Christophe and J. Inglada, "Robust Road Extraction for High Resolution Satellite Images", Proceedings of ICIP 2007, pp. 437 - 440.
- [21] A. Grote, C. Heipke, "Road extraction for the update of road databases in suburban areas", The International Archives of the Photogrammetry, Remote Sensing and Spatial Information Sciences. Vol. XXXVII. Part B3b, pp. 563-568, 2008.
- [22] J. Shi and J. Malik, "Normalized cuts and image segmentation", IEEE Transactions on Pattern Analysis and Machine Intelligence, Vol. 22, No. 8, pp. 888-905, 2000.
- [23] A. Zlotnick and P. Carnine, "Finding roads seeds in aerial images", CVGIP: Image Understanding 57: 243-260, 1993.
- [24] L. Tang, W. Xie and J. Huang, "Finding main road seeds on symmetrical edge orientation histogram", Electronics Lett., Vol. 40, No. 4, 2004.
- [25] V. Pandit, S. Gupta and K. S. Rajan, "Automatic road network extraction using high resolution multi-temporal satellite images", Proceedings of IEEE IGARSS 2009.

- [26] V. Pandit and K. S. Rajan, “Adaptive texture matching for road extraction”, Submitted for peer review to IEEE Transactions on Image Processing.
- [27] J. Sklansky, “Image segmentation and feature extraction”, System Man. Cybemat 8, pp. 237-247, 1978.
- [28] V. Castelli and L. Bergman, Image databases: search and retrieval of digital imagery, Wiley and sons, New York, 2002.
- [29] H. Tamura, S. Mori, and T. Yamawaki, “Texture features corresponding to visual perception”, IEEE Trans. Sys. Man. Cyb. SMC-8(6), 780-786 (1978).
- [30] R. Haralick and L. Shapiro, Computer and Robot Vision vol I, Addison-Wesley 1992, Appendix A.
- [31] D. McKeown and J. Denlinger, “Cooperative methods for road tracking in aerial imagery”, in Proc. CVPR, 1988, pp. 662672.
- [32] T. Deselaers, D. Keysers and H. Ney, “FIRE - Flexible Image Retrieval Engine: ImageCLEF 2004 Evaluation”, Proc. CLEF 2004 Workshop, pp. 535-544, 2004.
- [33] Q. Li, H. Hu and Z. Shi, “Semantic feature extraction using genetic programming in image retrieval”, Proceedings of ICPR, Vol. 1, pp. 648-651, 2004.
- [34] Q. Li, Z. Shi and S. Luo, “A neural network approach for bridging the semantic gap in texture image retrieval”, Proceedings of International Joint Conference on Neural Networks, pp. 581-585, 2007.
- [35] Y. Wei, S. Bhandarkar and K. Li, Semantics based video indexing using a stochastic modeling approach”, Proceeding of ICIP, Vol. 4, pp. 313-316, 2007.
- [36] F. Yali, C. Kui, “Indexing wood image for retrieval based on Kansei factors”, Proceeding of ICSP, pp. 1099-1102, 2008.
- [37] G. Seber, Multivariate Observations, Wiley, New York, 1984.
- [38] H. Spath, (1985) Cluster Dissection and Analysis: Theory, FORTRAN Programs, Examples, translated by J. Goldschmidt, Halsted Press, New York, 226 pp.
- [39] M. Flickner, “Query by image and video content”. The QBIC system, IEEE Comput. 28(9), 23 - 32 (1995).
- [40] Implementation of Tamura features. [Online]. Available: http://en.pudn.com/downloads123/sourcecode/graph/texture_mapping/d
- [41] C. Wiedemann, C. Heipke and H. Mayer, “Empirical evaluation of automatically extracted road axes”, Proc. CVPR Workshop Empirical Eval. Methods Comput. Vis., Los Alamitos, CA, pp. 172187, 1998.
- [42] V. Pandit and K. S. Rajan, “Potential applications of high resolution multi-temporal imageries”, ISRS Symposium 2009.